Supporting Information for

Tandem Scholl Reaction for the Synthesis of Twisted Nanographenes

Zixian Wu,[a] Zheng Zhou,[b] Yuanjian Zhang [a] and Yong Yang [a]*

[a]*School of Chemistry and Chemical Engineering, Southeast University, Nanjing 211189, Jiangsu, China*

[b]*School of Materials Science and Engineering, Tongji University, Shanghai 201804, China*

*Email: yonyan@seu.edu.cn

General S2

Materials S2

Literature review on the tandem Scholl reaction S3

Synthesis S5

X-ray crystallography S25

The mechanism of the Scholl reaction S29

Thermal isomerization of **4b** S31

Photophysical property S32

DFT calculation S34

Reference S41

General

The silica-gel column chromatography was performed using Greagent silica gel (300–400 mesh). The nuclear magnetic resonance (NMR) measurements were performed on NMR spectrometers operating at 400 MHz or 600 MHz proton frequencies at 25 °C. Standard pulse sequences were used. Chemical shifts (δ) are reported in parts per million (ppm) relative to the solvent residual peak (^{1}H and ^{13}C NMR, respectively): $CDCl_3$ (δ = 7.26 and 77.16 ppm) and CD_2Cl_2 (δ = 5.32 and 53.84 ppm). High-resolution mass spectrometry (HRMS) measurements were performed by the mass-spectrometry service at Shanghai Institute of Organic Chemistry, Chinese Academy of Science. For all reactions performed at elevated temperatures, oil bath was used as a heat source.

Materials

Anhydrous solvents and chemical reagents were purchased from commercial sources and used without further purification unless stated otherwise. 2-[4,4'-di-*tert*-butyl-(1,1'-biphenyl)-2-yl]-4,4,5,5-tetramethyl-1,3,2-dioxaborolane was prepared according to literature method.[1] The reactions were performed under N_2 atmosphere unless stated otherwise.

Literature review on the tandem Scholl reaction

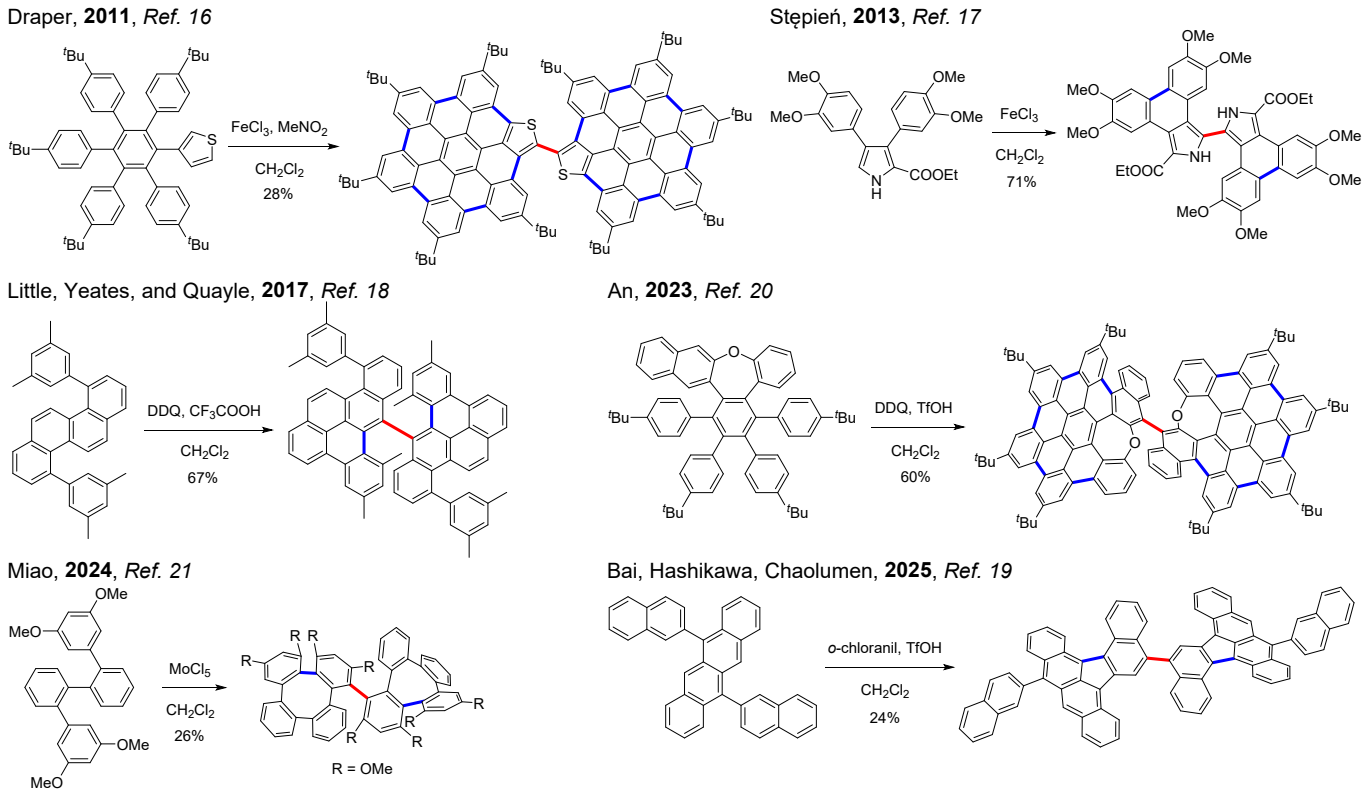

Scheme S1. Selected examples of the tandem Scholl reaction for the synthesis of polycyclic nanocarbons. The C–C bonds highlighted in blue and red indicate the intra- and intermolecular coupling, respectively.

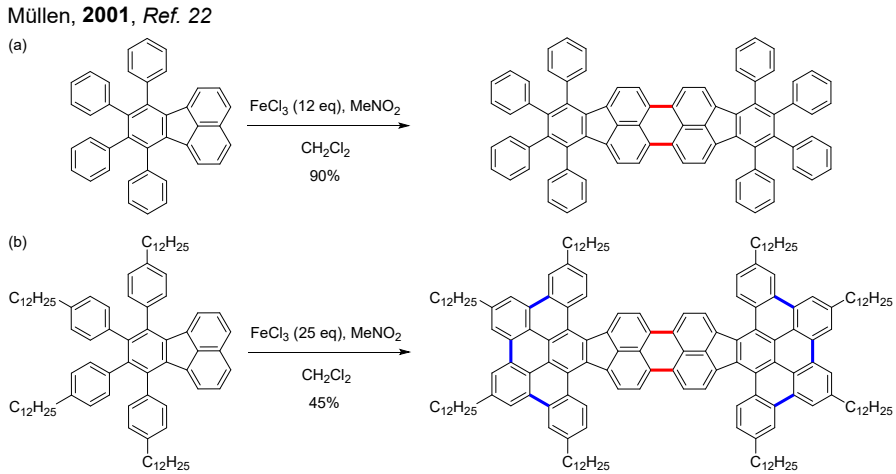

Scheme S2. An example of the tandem Scholl reaction that enables the formation of multiple intramolecular C–C bonds and two intermolecular C–C bonds. The C–C bonds highlighted in blue and red indicate the intra- and intermolecular coupling, respectively.

(a) Wang, **2023**, *Ref. 33*

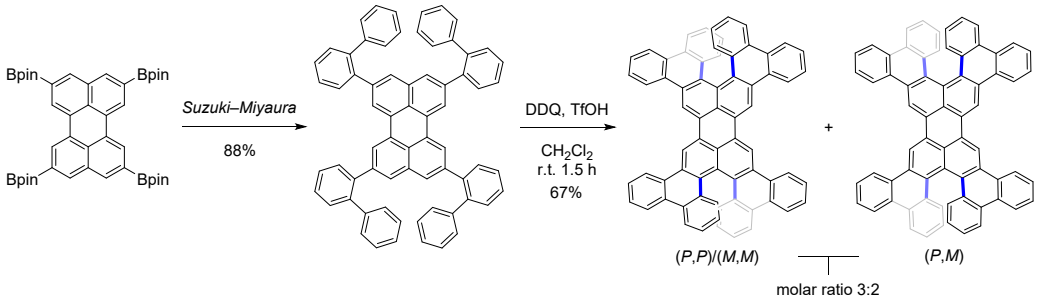

(b) Pradhan, **2024**, *Ref. 32*

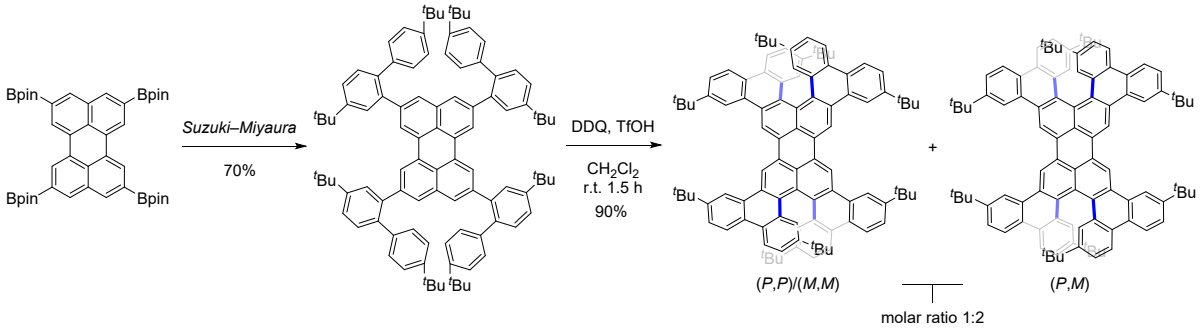

Scheme S3. Synthesis of (b) **2** and (a) its unsubstituted analog by the Scholl reaction reported in the literature.

Synthesis

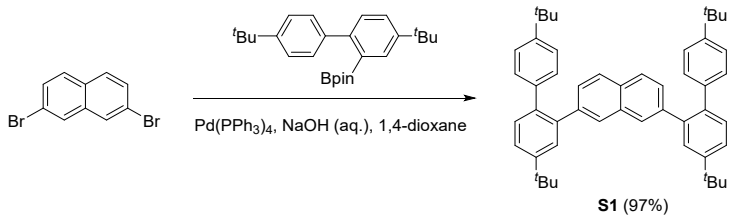

S1 (97%)

A mixture of 2,7-dibromonaphthalene (81.7 mg, 0.286 mmol), 2-[4,4'-di-*tert*-butyl-(1,1'-biphenyl)-2-yl]-4,4,5,5-tetramethyl-1,3,2-dioxaborolane (280 mg, 0.714 mmol), $Pd(PPh_3)_4$ (41.3 mg, 0.0357 mmol), NaOH (2M aq.; 0.72 mL, 1.43 mmol), and 1,4-dioxane (6 mL) was stirred at 80 °C for 16 h. The mixture was diluted with DCM, washed with water and brine, dried over anhydrous $MgSO_4$ and concentrated under reduced pressure. The crude product was purified by silica-gel column chromatography using petroleum ether/ethyl acetate (40:1 v/v) as an eluent to afford **S1** in 97% yield (182 mg, 0.277 mmol) as a white solid. ^{1}H NMR (600 MHz, $CDCl_3$, ppm): δ 7.73 (s, 2H), 7.53 (d, J = 8.4 Hz, 2H), 7.51 (s, 2H), 7.47 (d, J = 8.2 Hz, 2H), 7.42 (d, J = 7.9 Hz, 2H), 7.20 (d, J = 8.0 Hz, 4H), 7.11 (d, J = 8.0 Hz, 6H), 1.41 (s, 18H), 1.27 (s, 18H). ^{13}C NMR (150 MHz, $CDCl_3$, ppm): δ 150.4, 149.3, 140.3, 140.1, 138.4, 137.9, 133.6, 130.7, 130.6, 129.7, 128.7, 128.5, 128.3, 126.7, 124.9, 124.7, 34.8, 34.5, 31.6, 31.5. HRMS (ESI) *m/z*: $[M+H]^+$ Calcd. for $C_{50}H_{57}$ 657.4455; Found 657.4448.

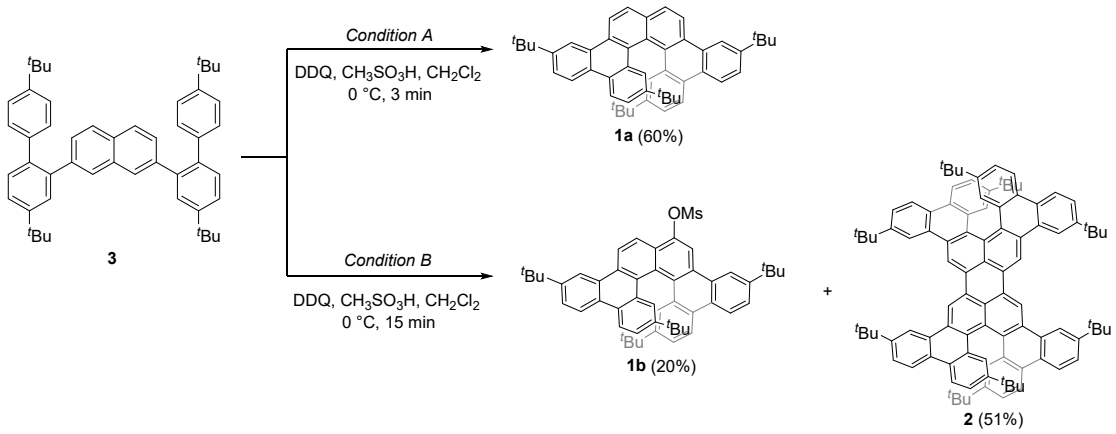

Condition A: To a mixture of **S1** (20.0 mg, 0.0304 mmol) and DDQ (27.6 mg, 0.122 mmol) in 1.8 mL of anhydrous CH_2Cl_2 was dropwise added CH_3SO_3H (0.18 ml) at 0 °C, and the resultant mixture was stirred at room temperature for 3 min. The reaction was quenched with saturated $NaHCO_3$ solution. The organic phase was separated, washed with saturated $NaHCO_3$ solution and brine, dried over anhydrous $MgSO_4$ and concentrated under reduced pressure. The crude product was purified by silica-gel column chromatography using petroleum ether/CH_2Cl_2 (15:1 v/v) as an eluent to afford **1a** in 60% yield (11.8 mg, 0.0182 mmol) as

a white solid. ^{1}H NMR (600 MHz, $CDCl_3$, ppm): δ 8.78 (d, *J* = 8.5 Hz, 2H), 8.71 (s, 2H), 8.54 (d, *J* = 8.5 Hz, 2H), 8.35 (d, *J* = 8.6 Hz, 2H), 8.13 (d, *J* = 8.4 Hz, 2H), 7.77 (d, *J* = 8.5 Hz, 4H), 7.62 (s, 2H), 7.29 (d, *J* = 8.5 Hz, 2H), 1.57 (s, 18H), 0.70 (s, 18H). ^{13}C NMR (150 MHz, $CDCl_3$, ppm): δ 149.5, 147.9, 133.0, 129.7, 129.4, 129.35, 129.30, 128.5, 127.3, 127.1, 125.3, 125.1, 124.9, 124.7, 122.8, 122.5, 121.6, 119.9, 35.3, 34.2, 31.7, 30.8. HRMS (ESI) *m/z*: $[M+Na]^+$ Calcd. for $C_{50}H_{52}Na$ 675.3961; Found 675.3967.

Condition B: To a mixture of **S1** (68.8 mg, 0.105 mmol) and DDQ (95.1 mg, 0.419 mmol) in 1.0 mL of anhydrous CH_2Cl_2 was dropwise added CH_3SO_3H (0.10 ml) at 0 °C, and the resultant mixture was stirred at 0 °C for 15 min. The reaction was quenched with saturated $NaHCO_3$ solution. The organic phase was separated, washed with saturated $NaHCO_3$ solution and brine, dried over anhydrous $MgSO_4$ and concentrated under reduced pressure. The crude product was purified by silica-gel column chromatography using petroleum ether/CH_2Cl_2 (10:1 v/v) as an eluent to afford **2** in 51% yield (34.9 mg, 0.0268 mmol) as a red solid and then petroleum ether/ethyl acetate (10:1 v/v) as an eluent to afford **1b** in 20% yield (15.7 mg, 0.0210 mmol) as a white solid. **1b**: ^{1}H NMR (600 MHz, $CDCl_3$, ppm): δ 8.88 (d, *J* = 8.8 Hz, 1H), 8.80 (s, 1H), 8.71 (s, 1H), 8.59 (s, 1H), 8.54 (d, *J* = 8.5 Hz, 2H), 8.45 (d, *J* = 8.6 Hz, 1H), 8.35 (dd, *J* = 8.8 Hz, 2.6 Hz, 2H), 7.81 (d, *J* = 8.5 Hz, 2H), 7.53 (dd, *J* = 4.6 Hz, 2.0 Hz, 2H), 7.31 (dd, *J* = 8.6 Hz, 2.0 Hz, 2H), 3.36 (s, 3H), 1.58 (s, 18H), 0.70 (s, 18H). ^{13}C NMR (150 MHz, $CDCl_3$, ppm): δ 150.0, 149.9, 148.24, 148.20, 144.6, 130.2, 129.4, 129.3, 129.1, 128.9, 128.8, 128.69, 128.67, 128.6, 127.6, 127.5, 126.6, 126.5, 126.1, 125.9, 125.18, 125.16, 125.0, 124.9, 122.91, 122.86, 122.7, 122.6, 120.0, 119.94, 119.87, 114.1, 38.1, 35.3, 34.2, 31.70, 31.67, 30.7. HRMS (ESI) *m/z*: $[M+H]^+$ Calcd. for $C_{51}H_{55}O_3S$ 747.3866; Found 747.3853.

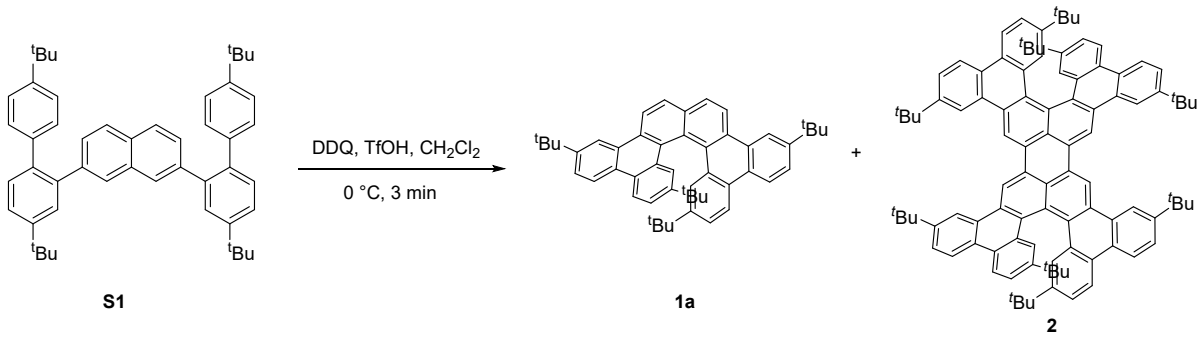

S1 **1a** **2**

To a mixture of **S1** (78.5 mg, 0.119 mmol) and DDQ (108 mg, 0.467 mmol) in 3.0 mL of anhydrous CH_2Cl_2 was dropwise added TfOH (0.03 ml) at 0 °C, and the resultant mixture was stirred at 0 °C for 3 min. The reaction was quenched with saturated $NaHCO_3$ solution. The organic phase was separated, washed with saturated $NaHCO_3$ solution and brine, dried over anhydrous $MgSO_4$ and concentrated under reduced

pressure. The crude product was purified by silica-gel column chromatography using petroleum ether/CH_2Cl_2 (15:1 v/v) as an eluent to afford **1a** in 30% yield (23.3 mg, 0.0367 mmol) as a white solid and afford **2** in 24% yield (18.6 mg, 0.0143 mmol) as a red solid.

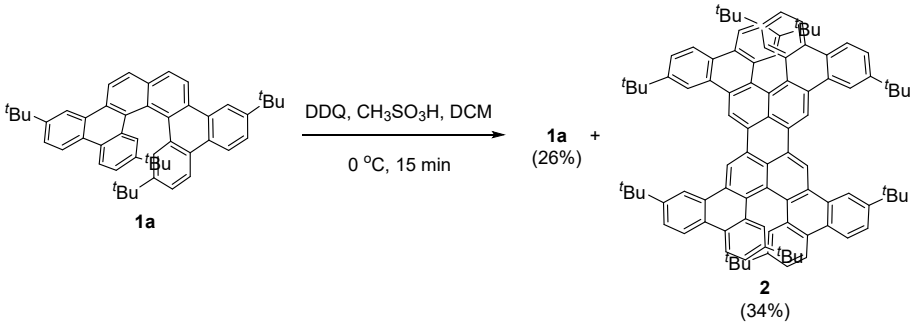

To a mixture of **1a** (58.5 mg, 0.0896 mmol) and DDQ (40.7 mg, 0.179 mmol) in 4.5 mL of anhydrous CH_2Cl_2 was dropwise added CH_3SO_3H (0.45 ml) at 0 °C, and the resultant mixture was stirred at 0 °C for 15 min. The reaction was quenched with saturated $NaHCO_3$ solution. The organic phase was separated, washed with saturated $NaHCO_3$ solution and brine, dried over anhydrous $MgSO_4$ and concentrated under reduced pressure. The crude product was purified by silica-gel column chromatography using petroleum ether/CH_2Cl_2 (15:1 v/v) as an eluent to recover **1a** in 27% yield (16 mg, 0.0245 mmol) as a white solid and afford **2** in 34% yield (20 mg, 0.0154 mmol) as a red solid.

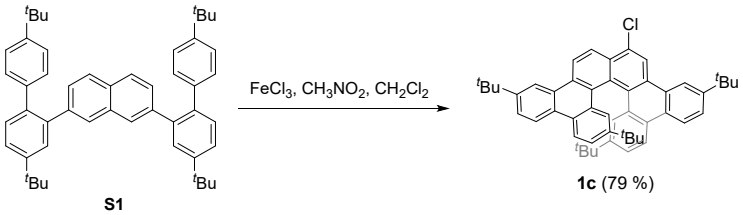

A solution of **S1** (131 mg, 0.200 mmol) in 4 mL of anhydrous CH_2Cl_2 was bubbled with nitrogen for 5 min. To the above solution was added a suspension of iron(III) chloride (486 mg, 3.00 mmol) in 0.2 mL of nitromethane at 0 °C, and the resultant mixture was stirred at 0 °C for 30 min. The reaction was quenched with methanol, washed with water and brine, dried over anhydrous $MgSO_4$ and concentrated under reduced pressure. The crude product was purified by silica-gel column chromatography using petroleum ether/CH_2Cl_2 (10:1 v/v) as an eluent to afford **1c** (108 mg, 0.158 mmol) in 79% yield as a yellow solid. ^{1}H NMR (600 MHz, $CDCl_3$, ppm): δ 8.87 (d, J = 9.0 Hz, 1H), 8.83 (s, 1H), 8.72 (s, 1H), 8.61-8.60 (m, 2H), 8.54 (d, J = 5.5 Hz, 1H), 8.52 (d, J = 5.6 Hz, 1H), 8.34 (d, J = 6.3 Hz, 1H), 8.32 (d, J = 6.9 Hz, 1H), 7.79 (d, J = 8.2 Hz, 2H), 7.52-7.51 (m, 2H), 7.28 (dd, J = 8.5 Hz, 2.0 Hz, 2H), 1.58 (s, 18H), 0.69 (s, 9H), 0.68 (s, 9H). ^{13}C NMR (150 MHz, $CDCl_3$, ppm): δ 149.9, 149.8, 148.2, 148.1, 131.3, 130.2, 129.9, 129.5,

129.37, 129.35, 129.1, 128.9, 128.7, 128.5, 128.3, 127.5, 127.4, 126.7, 125.82, 125.77, 125.0, 124.94, 124.85, 123.1, 122.9, 122.8, 122.5, 122.4, 121.7, 120.0, 119.8, 35.3, 34.2, 31.73, 31.71, 30.7. HRMS (APCI) *m*/*z*: $[M+H]^+$ Calcd. for $C_{50}H_{51}Cl$ 687.3752; Found 687.3740.

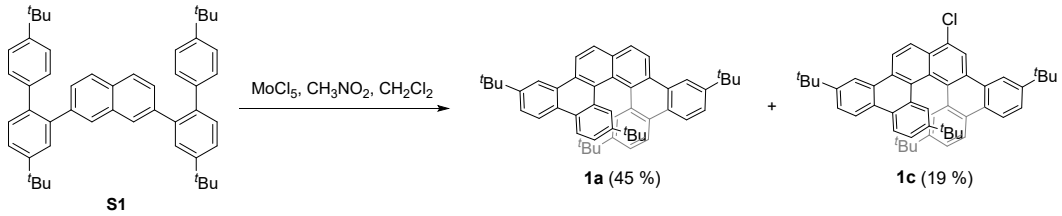

A solution of **S1** (65.7 mg, 0.100 mmol) in 2 mL of anhydrous CH_2Cl_2 was degassed by nitrogen bubbling for 5 min. To the degassed solution was added a suspension of molybdenum(V) chloride (410 mg, 1.50 mmol) in 0.1 mL of nitromethane, and the resultant mixture was stirred at room temperature for 2 h. The reaction was quenched with methanol, washed with water and brine, dried over anhydrous $MgSO_4$ and concentrated under reduced pressure. The crude product was purified by silica-gel column chromatography using petroleum ether/CH_2Cl_2 (10:1 v/v) as an eluent to afford **1a** (30.0 mg, 0.0454 mmol) in 45% yield as a white solid and **1c** (12.4 mg, 0.019 mmol) in 19% yield as a yellow solid, respectively.

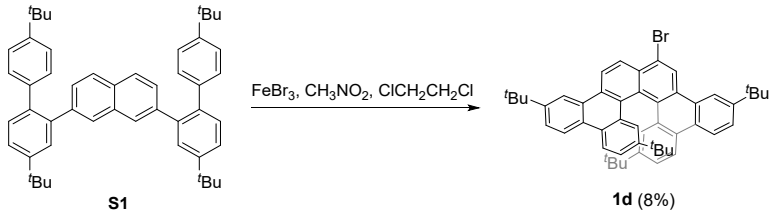

A solution of **S1** (131 mg, 0.200 mmol) in 4 mL of anhydrous $ClCH_2CH_2Cl$ was degassed by nitrogen bubbling for 5 min. To the degassed solution was added a suspension of iron(III) bromide (486 mg, 3.00 mmol) in 0.2 mL of nitromethane, and the resultant mixture was stirred at 80 ℃ for 1 h. The reaction was quenched with methanol, washed with water and brine, dried over anhydrous $MgSO_4$ and concentrated under reduced pressure. The crude product was purified by silica-gel column chromatography using petroleum ether/CH_2Cl_2 (10:1 v/v) as an eluent to afford **1d** (11.7 mg, 0.016 mmol) in 8% yield as a white solid. ^{1}H NMR (600 MHz, $CDCl_3$, ppm): δ 9.03 (s, 1H), 8.85 (d, *J* = 8.9 Hz, 1H), 8.72(s, 1H), 8.60 (s, 1H), 8.57 (d, *J* = 8.7 Hz, 1H), 8.53 (d, *J* = 8.4 Hz, 1H), 8.52 (d, *J* = 8.3Hz, 1H) , 8.33 (d, *J* = 7.9 Hz, 1H), 8.32 (d, *J* = 7.9 Hz, 1H), 7.79 (d, *J* = 8.3 Hz, 2H), 7.50 (s, 2H), 7.28 (d, *J* = 8.5 Hz, 2H), 1.57 (s, 18H), 0.69 (s, 9H), 0.68 (s, 9H). ^{13}C NMR (150 MHz, $CDCl_3$, ppm): δ 149.70, 149.57, 147.98, 147.85, 131.06, 129.66, 129.61, 129.09, 128.95, 128.84, 128.58, 128.49, 128.46, 127.87, 127.30, 127.19, 126.48, 125.73, 125.62,

125.57, 125.26, 124.80, 124.73, 124.60, 122.64, 122.60, 122.39, 122.29, 122.06, 119.75, 119.54, 35.14, 35.12, 33.93, 31.52, 31.49, 30.46. HRMS (APCI) *m/z*: $[M+H]^+$ Calcd. for $C_{50}H_{51}Br$ 731.3247; Found 731.3231.

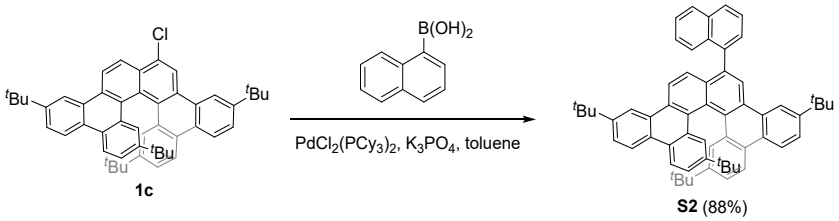

1c **S2** (88%)

A mixture of **1c** (180 mg, 0.262 mmol), 1-naphthylboronic acid (112mg, 0.656 mmol), $PdCl_2(PCy_3)_2$ (9.70 mg, 0.0131 mmol), K_3PO_4 (250 mg, 1.18 mmol), and toluene (3 mL) was stirred at 110 °C for 16 h. The mixture was diluted with DCM, washed with water and brine, dried over anhydrous $MgSO_4$ and concentrated under reduced pressure. The crude product was purified by silica-gel column chromatography using petroleum ether/CH_2Cl_2 (10:1 v/v) as an eluent to afford **S2** (180 mg, 0.231 mmol) in 88% yield as a white solid. This compound exists as a mixture of two stereoisomers possibly due to the restricted rotation of the 1-naphthyl unit, as indicated by the ^1H NMR spectrum. This compound was characterized by HRMS and used directly in the next step. HRMS (APCI) *m/z*: $[M+H]^+$ Calcd. for $C_{60}H_{58}$ 779.4611; Found 779.4605.

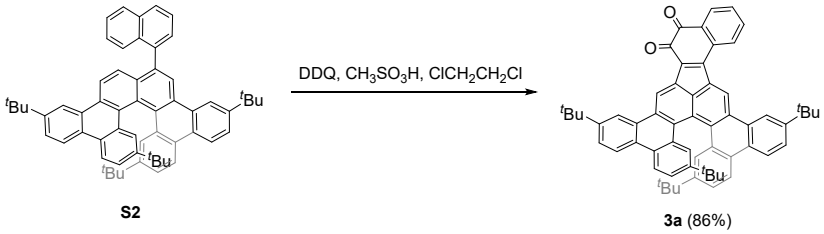

S2 **3a** (86%)

To a mixture of **S2** (37.7 mg, 0.0484 mmol) and DDQ (43.9 mg, 0.194 mmol) in 4.0 mL of anhydrous $ClCH_2CH_2Cl$ was dropwise added CH_3SO_3H (0.4 ml) at 0 °C, and the resultant mixture was stirred at 60 °C for 1 h. The reaction was quenched with saturated $NaHCO_3$ solution. The organic phase was separated, washed with saturated $NaHCO_3$ solution and brine, dried over anhydrous $MgSO_4$ and concentrated under reduced pressure. The crude product was purified by silica-gel column chromatography using petroleum ether/ethyl acetate (10:1 v/v) as an eluent to afford **3a** (33.6 mg, 0.0416 mmol) in 86% yield as a purple solid. ^1H NMR (600 MHz, $CDCl_3$, ppm) δ 9.77 (s, 1H), 9.75 (s, 1H), 8.89 (s, 1H), 8.78 (d, J = 1.9 Hz, 1H), 8.63 (d, J = 7.6 Hz, 1H), 8.61 (d, J = 8.5 Hz, 1H), 8.59 (d, J = 8.6 Hz, 1H), 8.44 (d, J = 6.8 Hz, 1H), 8.42 (d, J = 7.0 Hz, 1H), 8.30 (d, J = 7.6 Hz, 1H), 7.89 (t, J = 7.5 Hz, 1H), 7.86 (dd, J = 8.5, 1.8 Hz, 1H), 7.83

(dd, J = 8.6, 1.8 Hz, 1H), 7.79 (d, J = 2.0 Hz, 1H), 7.72 (d, J = 2.0 Hz, 1H), 7.61 (t, J = 7.6 Hz, 1H), 7.43 (dd, J = 8.4, 2.0 Hz, 1H), 7.39 (dd, J = 8.6, 2.1 Hz, 1H), 1.64 (s, 9H), 1.61 (s, 9H), 0.74 (s, 18H). ^{13}C NMR (101 MHz, $CDCl_3$, ppm): δ 181.7, 178.0, 150.5, 150.4, 148.9, 148.4, 147.7, 135.5, 135.03, 134.98, 132.93, 132.88, 132.86, 132.8, 132.4, 131.8, 131.4, 131.1, 130.2, 130.0, 129.9, 129.6, 129.4, 129.2, 128.9, 128.8, 128.6, 128.3, 128.2, 126.4, 126.3, 126.1, 126.0, 125.3, 124.9, 124.6, 124.1, 123.5, 123.2, 123.1, 122.9, 122.8, 120.4, 119.6, 35.5, 31.70, 31.69, 31.6, 30.8, 30.7, 30.3, 29.8. HRMS (APCI) m/z: $[M+Cl]^-$ Calcd. for $C_{60}H_{54}O_2$ 841.3818; Found 841.3824.

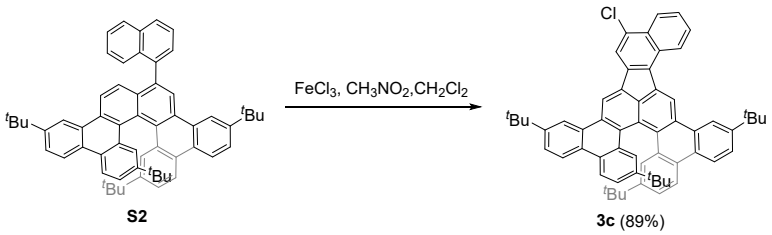

S2 **3c** (89%)

A solution of **S2** (30.4 mg, 0.039 mmol) in 2 mL of anhydrous CH_2Cl_2 was bubbled with nitrogen for 5 min. To the above solution was added a suspension of iron(III) chloride (94.4 mg, 0.585 mmol) in 0.1 mL of nitromethane, and the resultant mixture was stirred at 0 ℃ for 30 min. The reaction was quenched with methanol, washed with water and brine, dried over anhydrous $MgSO_4$ and concentrated under reduced pressure. The crude product was purified by silica-gel column chromatography using petroleum ether/CH_2Cl_2 (10:1 v/v) as an eluent to afford **3c** (28.1 mg, 0.0347 mmol) in 89% yield as a yellow solid. ^{1}H NMR (600 MHz, CD_2Cl_2, ppm) δ 9.75 (s, 1H), 9.31 (s, 1H), 9.07 (d, J = 8.3 Hz, 1H), 8.95 (s, 1H), 8.91 (s, 1H), 8.66 (d, J = 8.8 Hz, 1H), 8.65 (d, J = 8.8 Hz, 1H), 8.50 (s, 1H), 8.47 (dd, J = 8.6, 4.1 Hz, 2H), 8.44 (d, J = 8.3 Hz, 1H), 7.90-7.85 (m, 3H), 7.77 (dd, J = 10.0, 2.0 Hz, 2H), 7.68 (t, J = 7.6 , 1H), 7.41 (td, J = 8.5, 2.4 Hz, 2H), 1.67 (s, 9H), 1.65 (s, 9H), 0.743 (s, 9H), 0.736 (s, 9H). ^{13}C NMR (150 MHz, CD_2Cl_2, ppm): ^{13}C NMR (150 MHz, CD_2Cl_2) δ 150.5, 150.4, 148.72, 148.66, 138.6, 135.7, 134.8, 134.0, 133.7, 132.6, 132.5, 132.4, 131.8, 131.3, 130.9, 130.4, 130.3, 130.2, 129.5, 129.4, 129.3, 129.2, 128.65, 128.56, 128.52, 128.48, 127.0, 126.3, 125.9, 125.2, 125.0, 123.6, 123.3, 123.2, 123.0, 122.9, 121.1, 120.4, 120.3, 117.1, 35.63, 35.61, 34.5, 34.4, 31.79, 31.76, 30.8. HRMS (APCI) m/z: $[M+H]^+$ Calcd. for $C_{60}H_{55}Cl$ 811.4065; Found 811.4056.

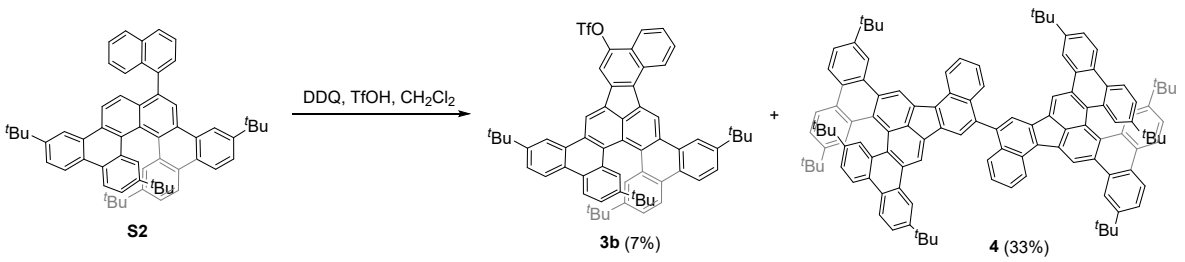

To a mixture of **S2** (251 mg, 0.323 mmol) and DDQ (293 mg, 1.29 mmol) in 5.0 mL of anhydrous CH_2Cl_2 was dropwise added TfOH (0.05 ml) at 0 °C, and the resultant mixture was stirred at 0 °C for 10 min. The reaction was quenched with saturated $NaHCO_3$ solution. The organic phase was separated, washed with saturated $NaHCO_3$ solution and brine, dried over anhydrous $MgSO_4$ and evaporated. The crude product was purified by silica-gel column chromatography using petroleum ether/CH_2Cl_2 (10:1 v/v) as an eluent to afford **3b** (20 mg 0.0216 mmol) in 7% yield as a yellow solid and **4** (81.1 mg, 0.0523 mmol) in 33% yield as a yellow solid, respectively. **4** was purified by silica-gel column chromatography repeatedly using petroleum ether/CH_2Cl_2 (10:1 v/v) as an eluent to afford **4a** (39.6 mg, 0.0255 mmol) and **4b** (32.4 mg, 0.0209 mmol).

3b: ^{1}H NMR (400 MHz, $CDCl_3$, ppm) δ 9.74 (s, 1H), 9.25 (s, 1H), 9.07 (d, J = 8.5 Hz, 1H), 8.88 (dd, J = 12.2, 1.9 Hz, 2H), 8.63 (d, J = 8.7 Hz, 1H), 8.62 (d, J = 8.7 Hz, 1H), 8.44 (dd, J = 8.7, 3.3 Hz, 2H), 8.32 (s, 1H), 8.24 (d, J = 8.4 Hz, 1H), 7.91-7.83 (m, 3H), 7.78 (t, J = 1.6 Hz, 2H), 7.71 (td, J = 7.7, 1.1 Hz, 1H), 7.40 (dd, J = 4.1, 2.1 Hz, 1H), 7.38 (dd, J = 4.1, 2.0 Hz, 1H), 1.67 (s, 9H), 1.66 (s, 9H), 0.75 (s, 9H), 0.74 (s, 9H). ^{13}C NMR (101 MHz, $CDCl_3$, ppm): δ 150.2, 150.0, 148.5, 148.4, 145.6, 137.8, 134.84, 134.81, 134.1, 133.5, 132.22, 132.19, 131.6, 130.9, 130.3, 130.02, 129.97, 129.1, 129.0, 128.8, 128.45, 128.40, 128.3, 127.2, 126.7, 125.7, 125.1, 125.0, 124.6, 123.3, 123.1, 123.0, 122.7, 122.6, 120.4, 120.1, 119.8, 117.4, 112.8, 35.5, 35.4, 34.32, 34.29, 31.9, 31.8, 30.82, 30.79. HRMS (APCI) *m*/*z*: $[M+H]^+$ Calcd. for $C_{60}H_{55}Cl$ 811.4065; Found 811.4056.

4a: ^{1}H NMR (400 MHz, $CDCl_3$, ppm) δ 9.86 (s, 1H), 9.85 (s, 1H), 9.33 (s, 1H), 9.29 (s, 1H), 9.20 (t, J = 9.2 Hz, 2H), 9.00 (d, J = 2.1 Hz, 2H), 8.81 (dd, J = 11.4, 2.0 Hz, 2H), 8.67 (d, J = 8.7 Hz, 2H), 8.62 (d, J = 11.2 Hz, 2H), 8.60 (t, J = 8.2 Hz, 2H), 8.48 (d, J = 8.6 Hz, 2H), 8.44 (t, J = 8.4 Hz, 2H), 7.89-7.75 (m, 12H), 7.50-7.35 (m, 6H), 1.71 (s, 18H), 1.52 (s, 9H), 1.49 (s, 9H), 0.78 (s, 9H), 0.77 (s, 27H). ^{13}C NMR (101 MHz, $CDCl_3$, ppm): δ 150.0, 149.95, 149.91, 149.89, 148.4, 148.3, 148.2, 141.9, 139.74, 139.72, 138.2, 138.1, 136.42, 136.40, 135.6, 135.5, 134.9, 134.8, 134.14, 134.09, 133.92, 133.88, 132.43, 132.39, 132.3, 132.2, 131.2, 131.1, 130.44, 130.43, 130.33, 130.30, 130.2, 129.92, 129.89, 129.4, 129.32, 129.29, 129.13, 129.11, 128.73, 128.71, 128.69, 128.5, 128.31, 128.29, 128.26, 128.2, 127.6, 126.0, 125.5, 125.42, 125.41, 124.8, 124.73, 124.68, 124.61, 124.59, 124.58, 123.52, 123.49, 123.1, 122.87, 122.86, 122.6, 122.5,

122.4, 120.1, 120.05, 119.98, 119.9, 116.58, 116.57, 35.5, 35.4, 35.3, 34.34, 34.31, 32.1, 31.83, 31.81, 31.76, 31.7, 31.6, 30.9, 30.3, 29.9, 29.8, 29.5. HRMS (APCI) *m*/*z*: $[M+H]^+$ Calcd. for $C_{120}H_{110}$ 1552.8714; Found 1552.8686.

4b: ^{1}H NMR (600 MHz, $CDCl_3$, ppm) δ 9.86 (s, 2H), 9.31 (s, *J* = 9.0 Hz, 2H), 9.00 (s, 2H), 8.82 (d, *J* = 2.0 Hz, 2H), 8.67 (d, *J* = 8.8 Hz, 2H), 8.61 (s, 2H), 8.60 (d, *J* = 10.1 Hz, 2H), 8.48 (d, *J* = 8.8 Hz, 2H), 8.44 (t, *J* = 9.0 Hz, 2H), 7.88 (dd, *J* = 8.7, 1.9 Hz, 2H), 7.86-7.83 (m, 8H), 7.78 (dd, *J* = 8.5, 2.0 Hz, 2H), 7.46 (t, *J* = 7.6 Hz, 2H), 7.41 (dd, *J* = 8.8, 2.0 Hz, 2H), 7.38 (dd, *J* = 8.4, 2.2 Hz, 2H), 1.70 (s, 18H), 1.52 (s, 18H), 0.78 (s, 18H), 0.77 (s, 18H). ^{13}C NMR was not collected due to the poor solubility and possible gradual isomerization of **4b** at room temperature. HRMS (APCI) *m*/*z*: $[M+H]^+$ Calcd. for $C_{120}H_{110}$ 1552.8714; Found 1552.8686.

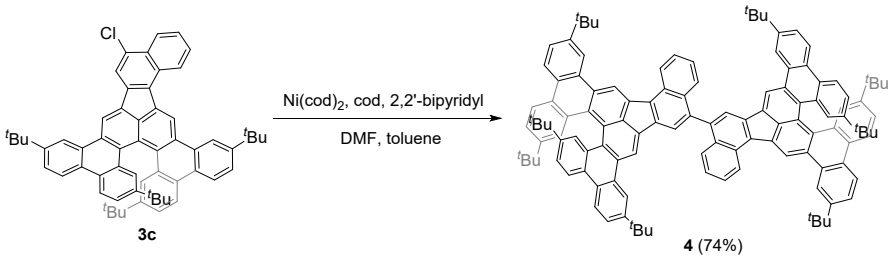

A mixture of $Ni(cod)_2$ (250 mg, 0.909 mmol), 1,5-cyclooctadiene (cod; 0.120 mL, 0.909 mmol), and 2,2'-bipyridyl (142 mg, 0.909 mmol) in toluene (0.5 mL) and DMF (0.5 mL) was stirred at 80 °C for 30 min. Then a solution of **3c** (18.4 mg, 0.0227 mmol) in toluene (2 mL) was dropwise added. The resultant mixture was stirred at 80 °C for 18 h. After the reaction mixture was cooled down to ambient temperature, hydrochloric acid (1M, 3 mL) was added. The mixture was diluted with DCM, washed with water and brine, dried over anhydrous $MgSO_4$ and concentrated under reduced pressure. The crude product was purified by silica-gel column chromatography using petroleum ether/CH_2Cl_2 (10:1 v/v) as an eluent to afford **4** in 74% yield (13 mg, 8.38 μmol) as a yellow solid.

Copies of NMR spectra

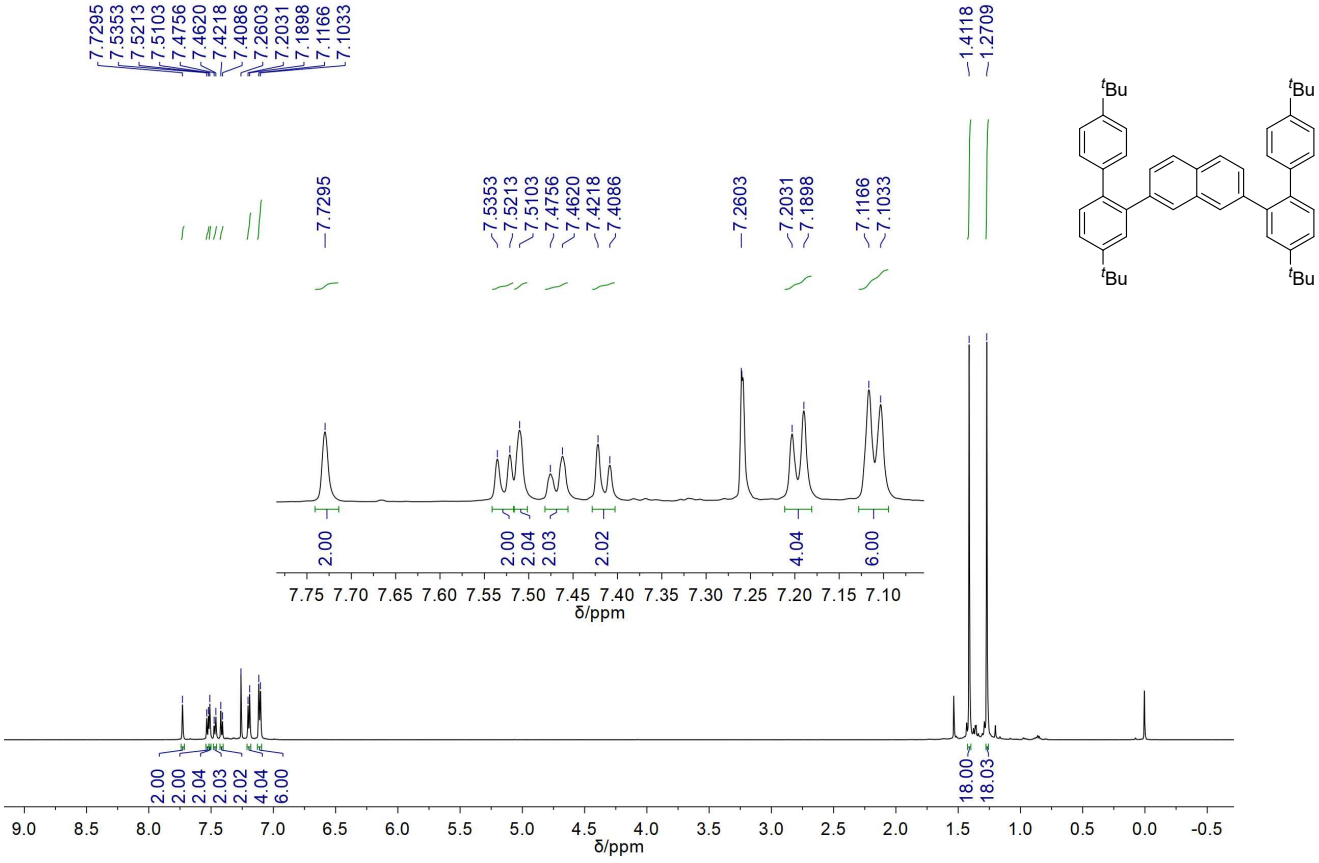

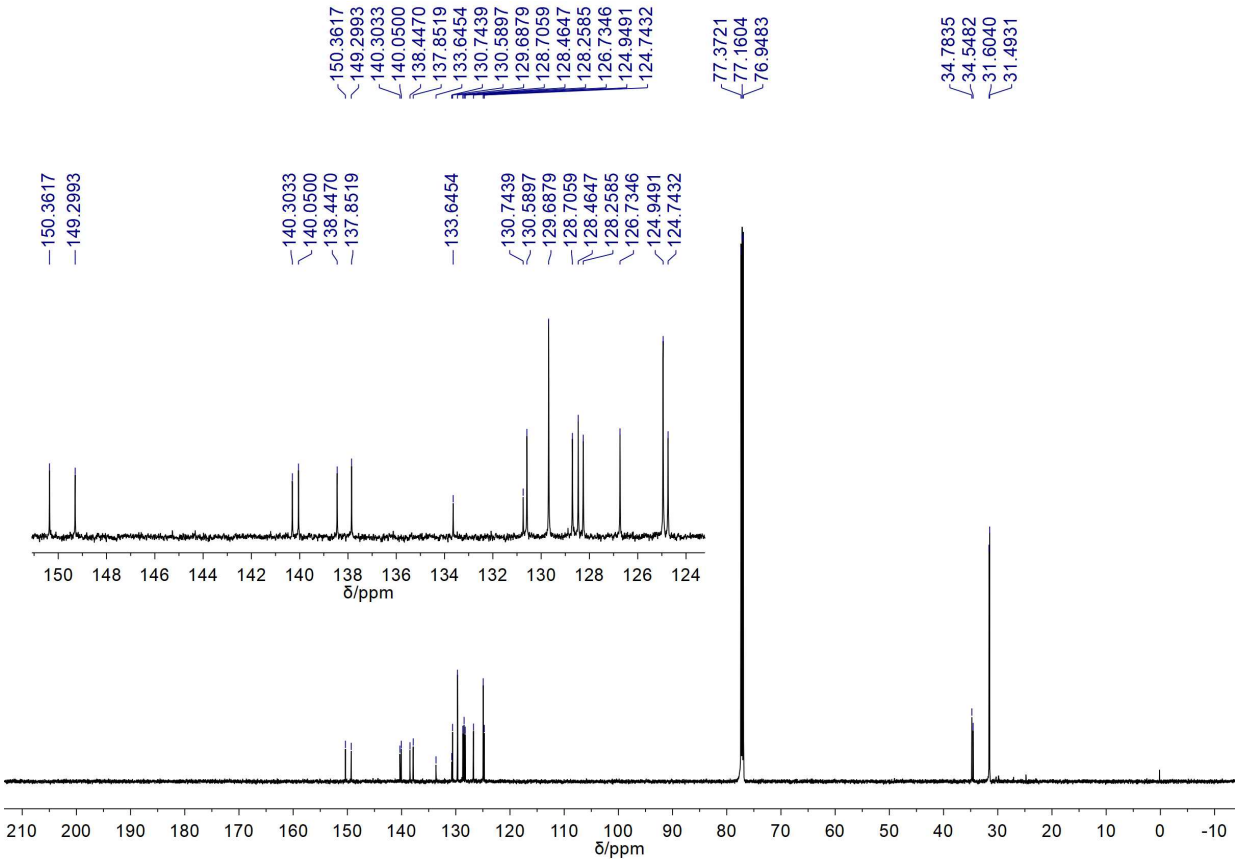

Figure S1. ^{1}H (600 MHz, top) and ^{13}C NMR (150 MHz, bottom) of **S1** in $CDCl_3$ at 25 °C.

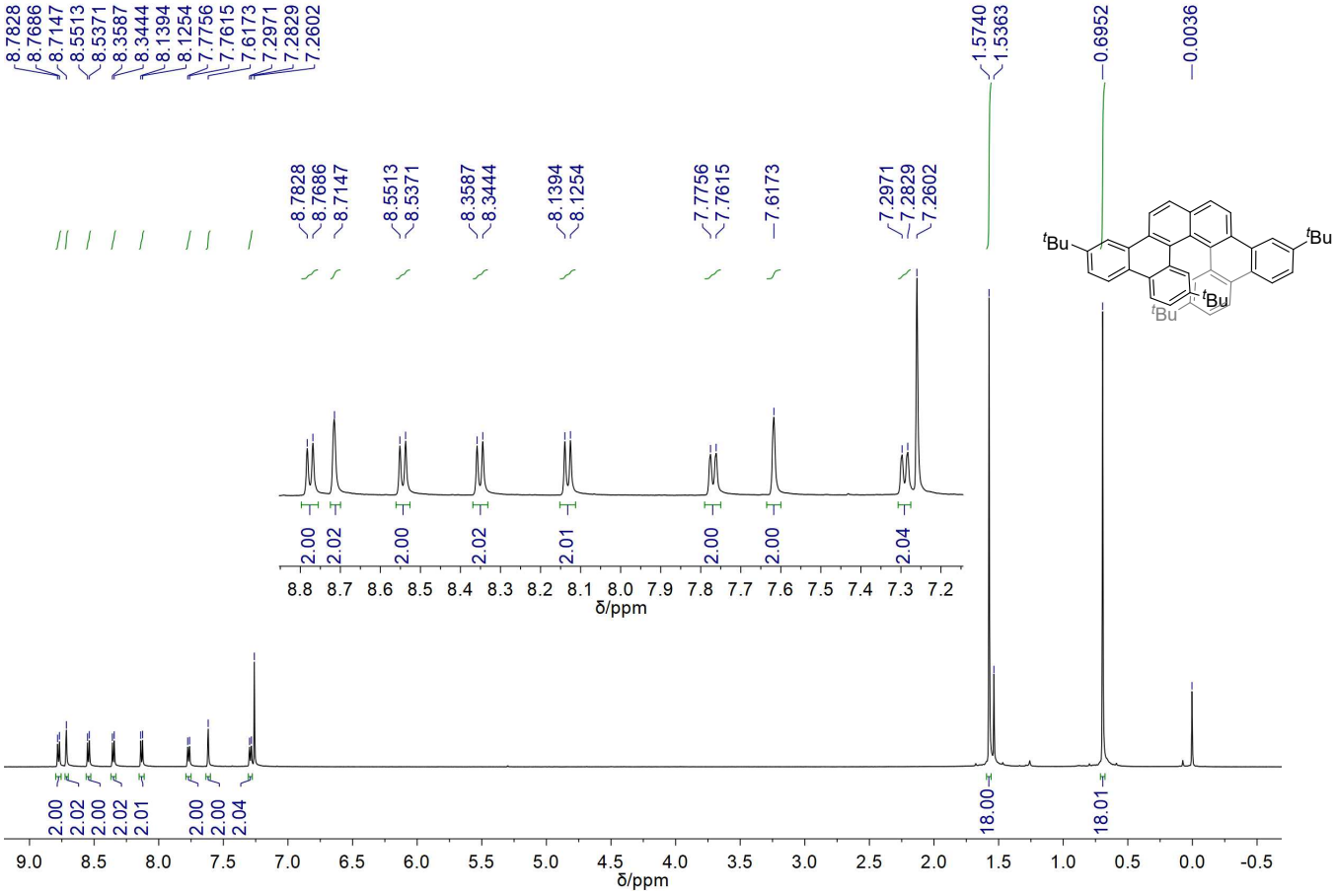

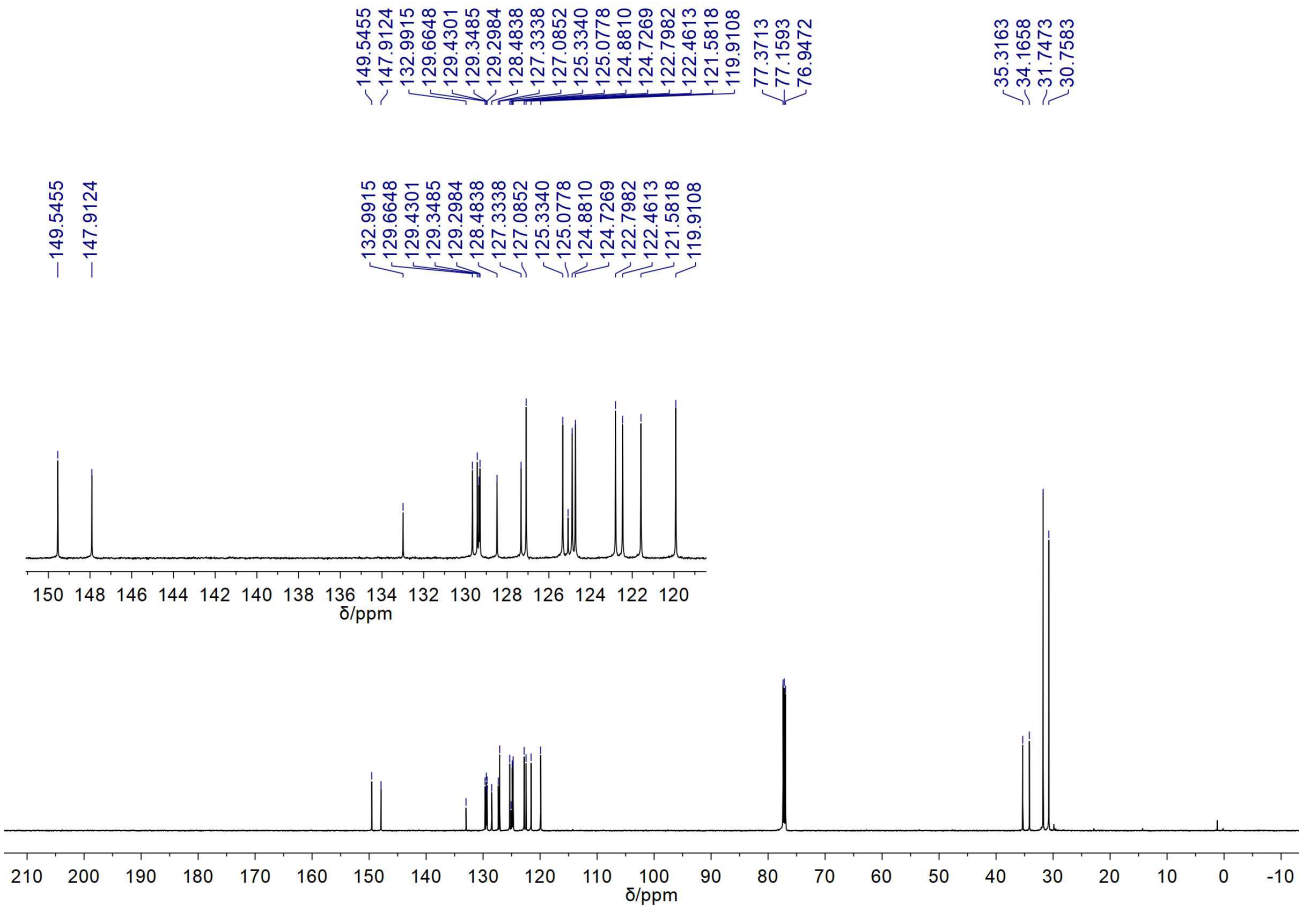

Figure S2. ^{1}H (600 MHz, top) and ^{13}C NMR (150 MHz, bottom) of **1a** in $CDCl_3$ at 25 °C.

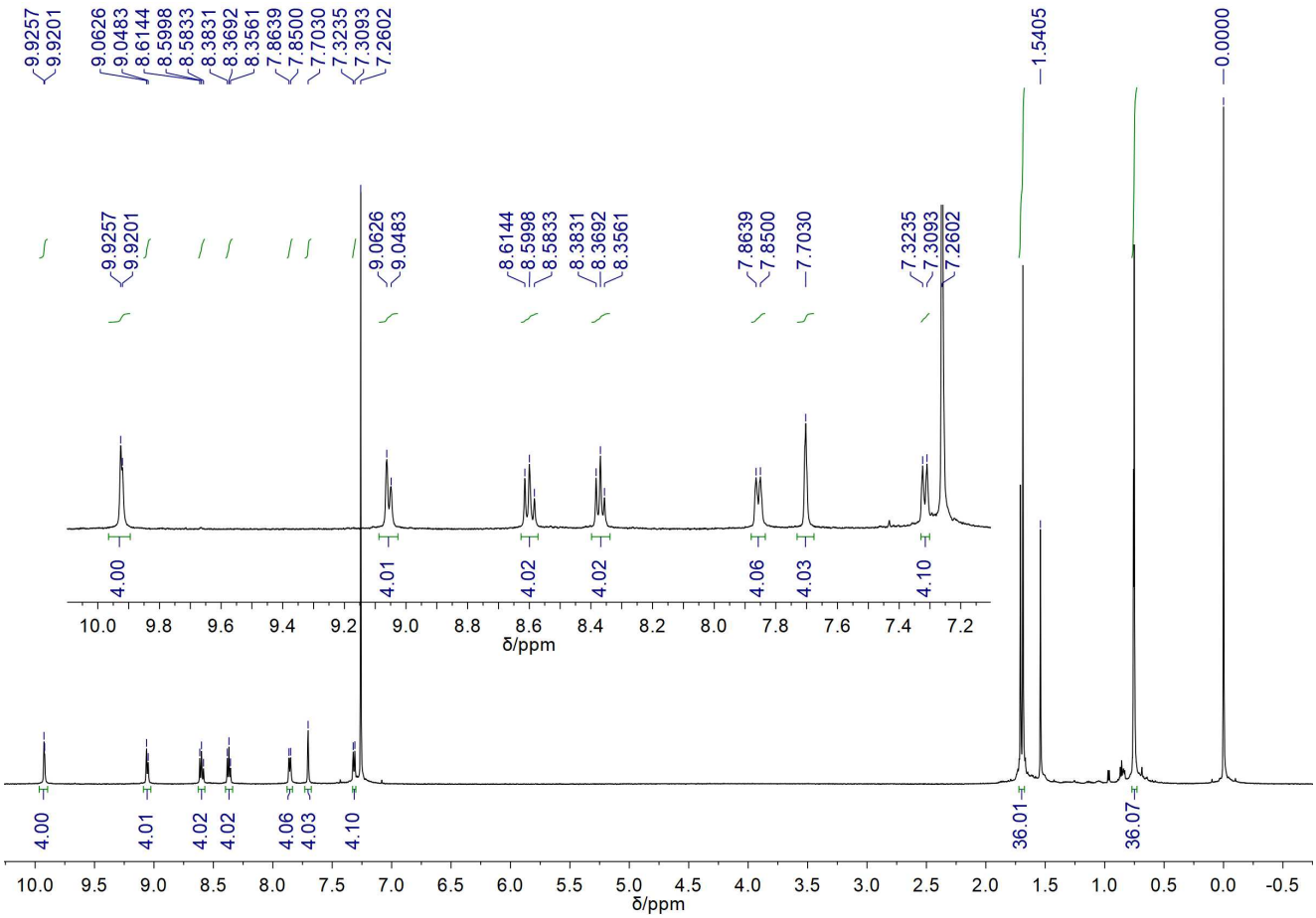

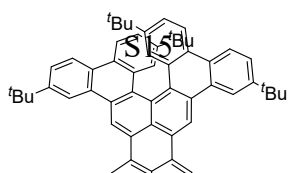

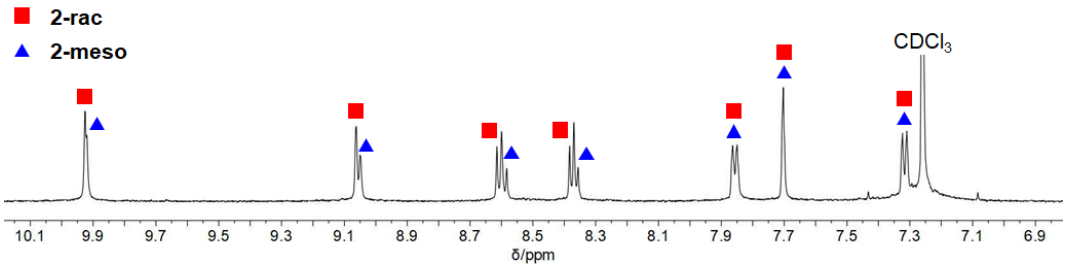

Figure S3. ^{1}H NMR (600 MHz) of **2** in $CDCl_3$ at 25 °C. The aromatic region is amplified for clarity.

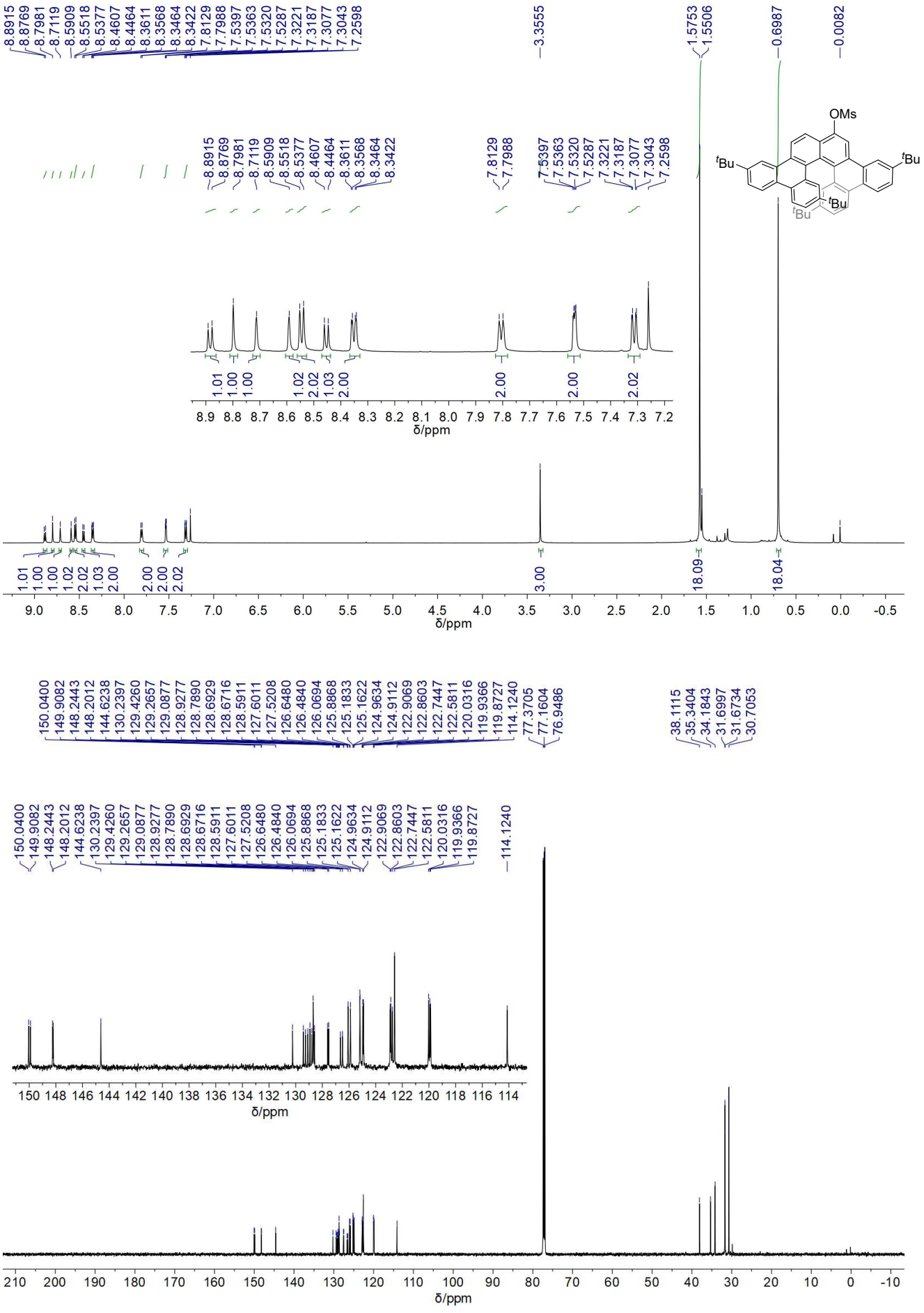

Figure S4. ^{1}H (600 MHz, top) and ^{13}C NMR (150 MHz, bottom) of **1b** in $CDCl_3$ at 25 °C.

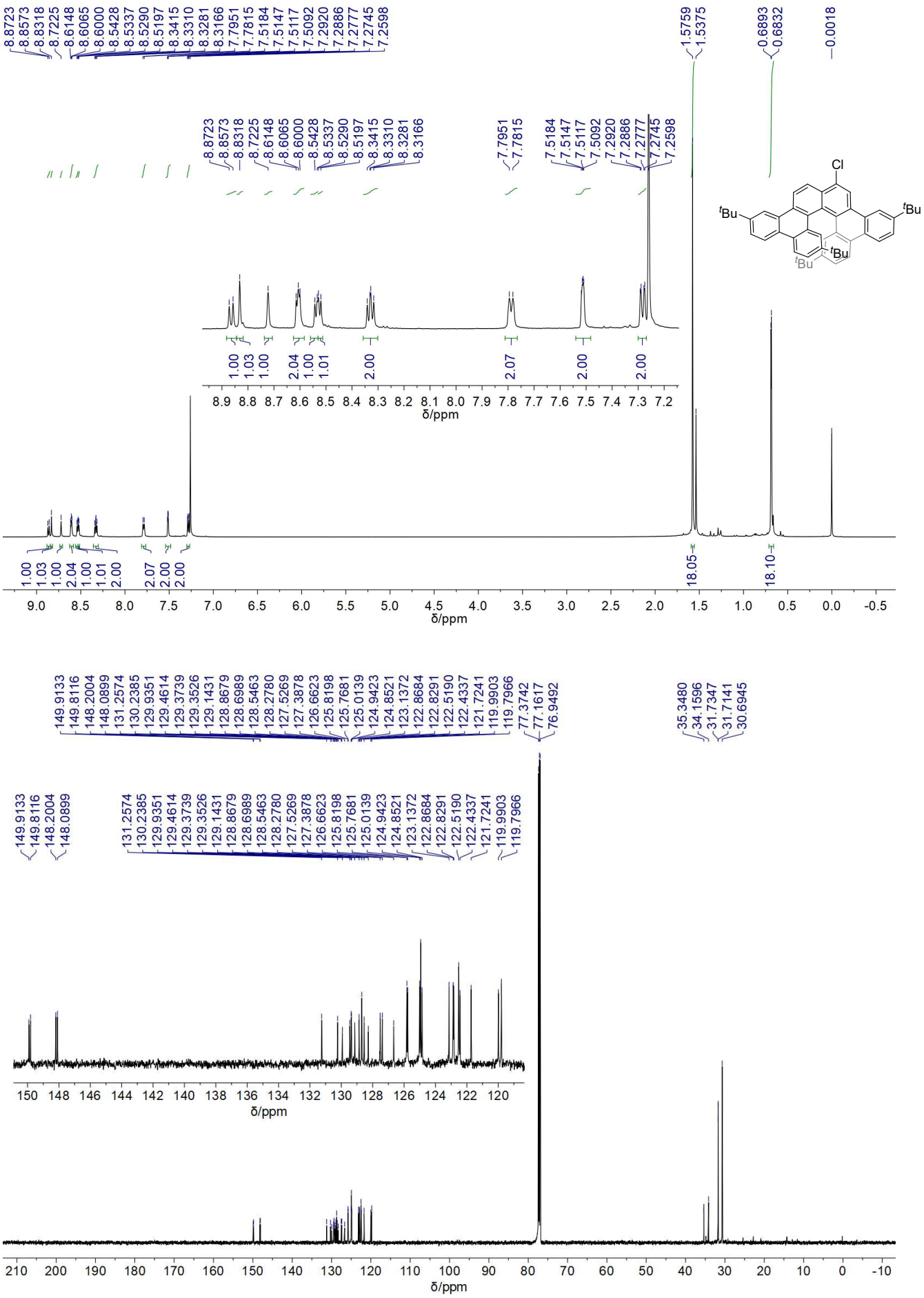

Figure S5. ^{1}H (600 MHz, top) and ^{13}C NMR (150 MHz, bottom) of **1c** in $CDCl_3$ at 25 °C.

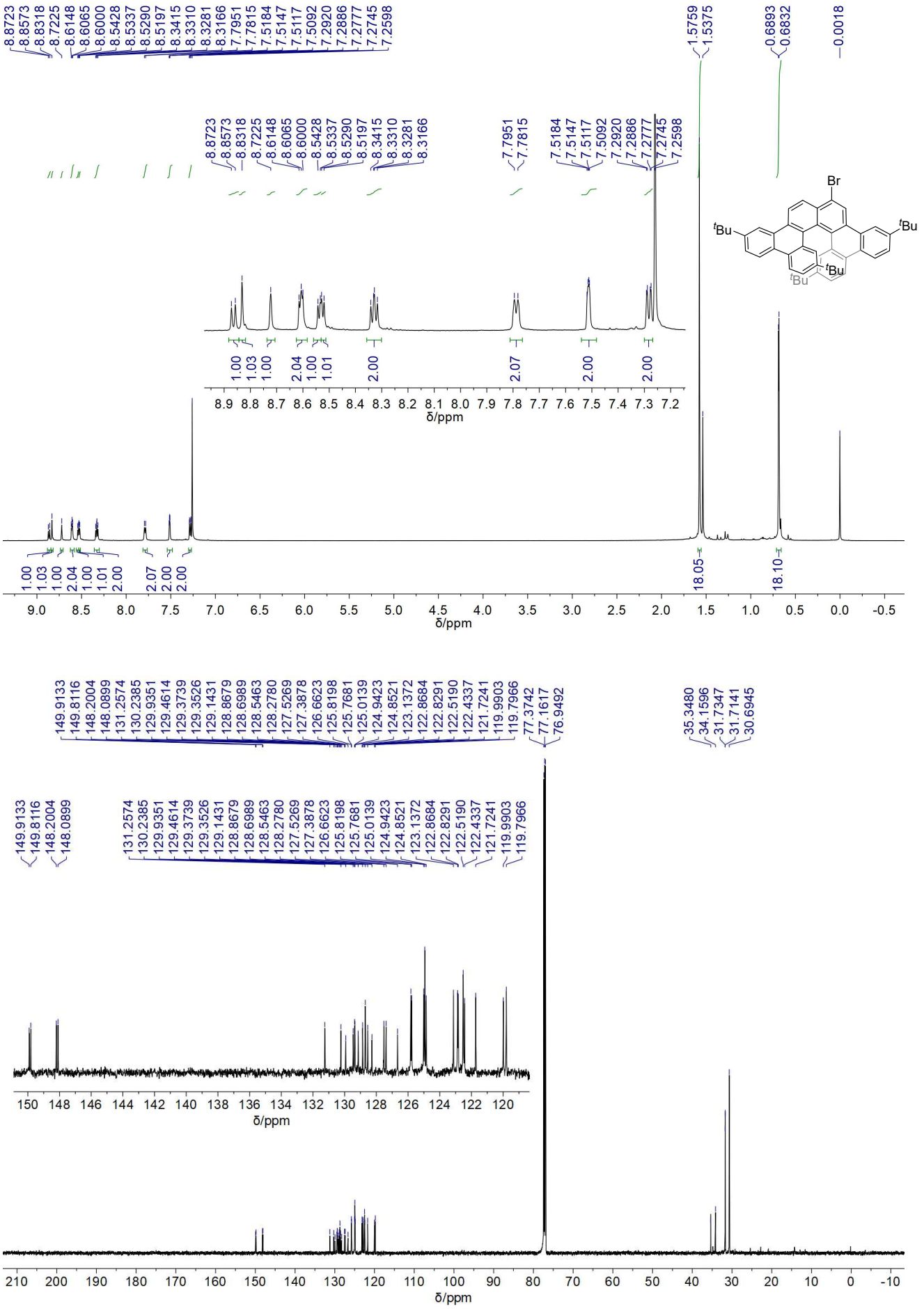

Figure S6. ^{1}H (600 MHz, top) and ^{13}C NMR (150 MHz, bottom) of **1d** in $CDCl_3$ at 25 °C.

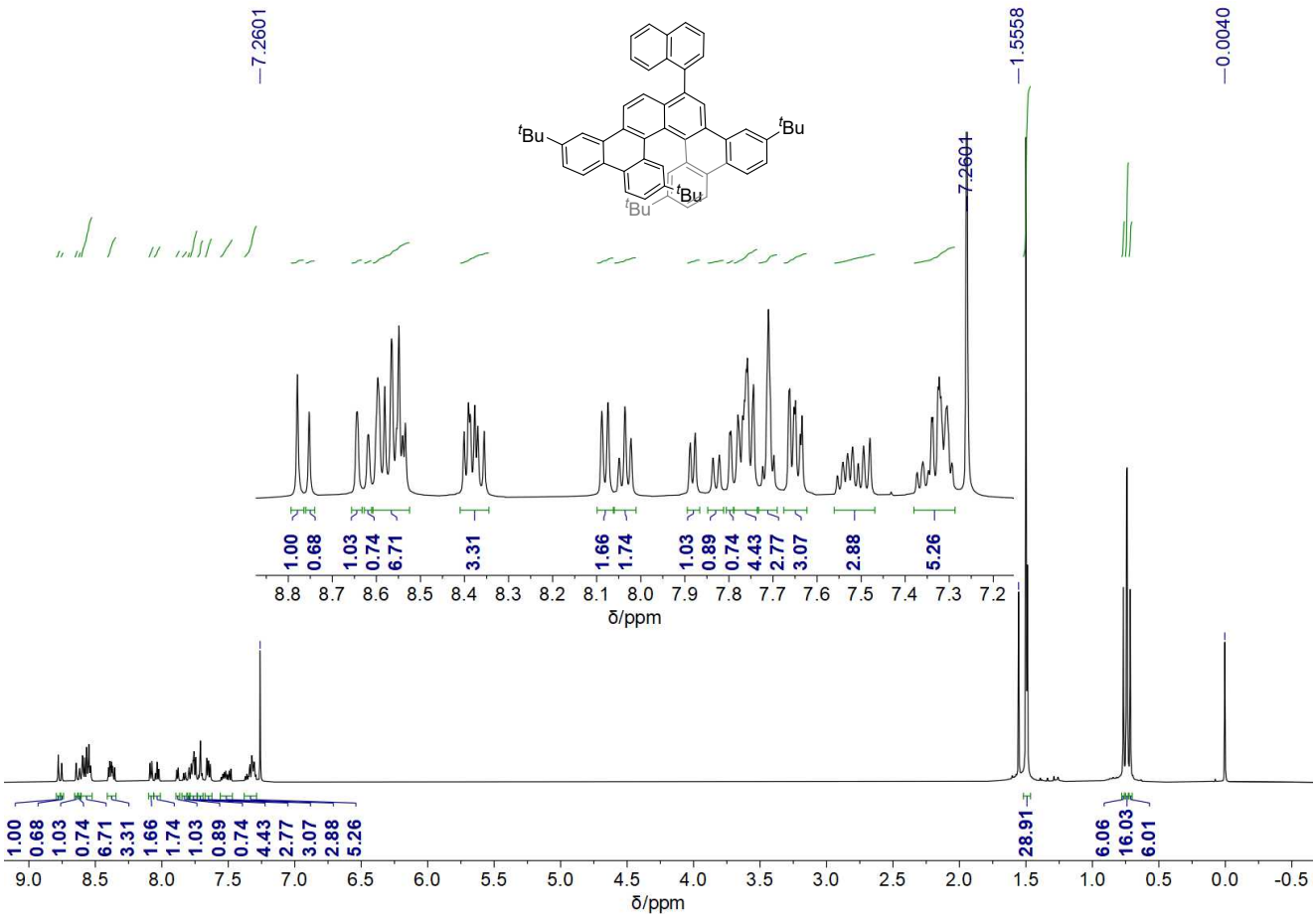

Figure S7. ^{1}H NMR (600 MHz, top) of **S2** in $CDCl_3$ at 25 °C.

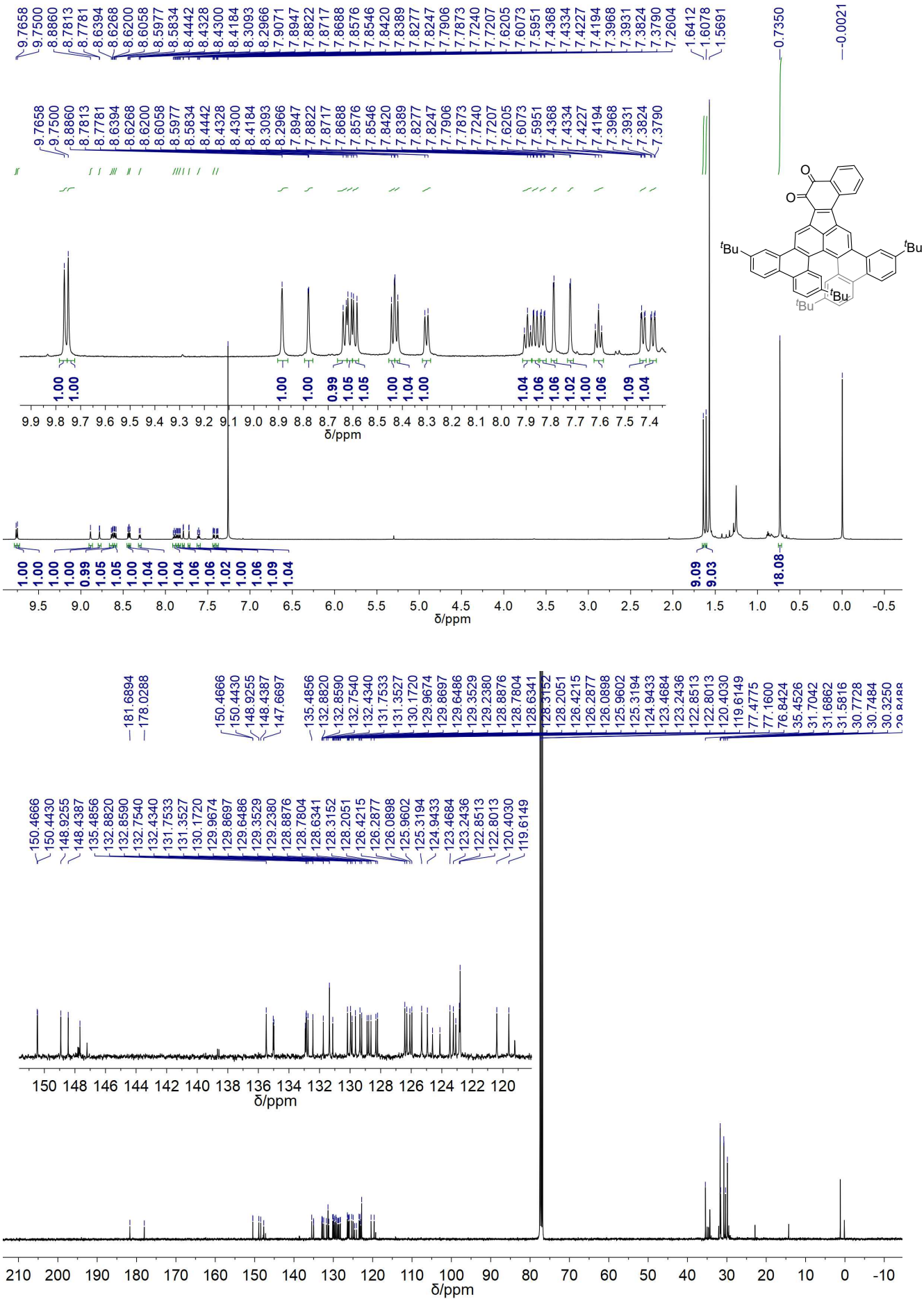

Figure S8. ^{1}H (600 MHz, top) and ^{13}C NMR (101 MHz, bottom) of **3a** in $CDCl_3$ at 25 °C.

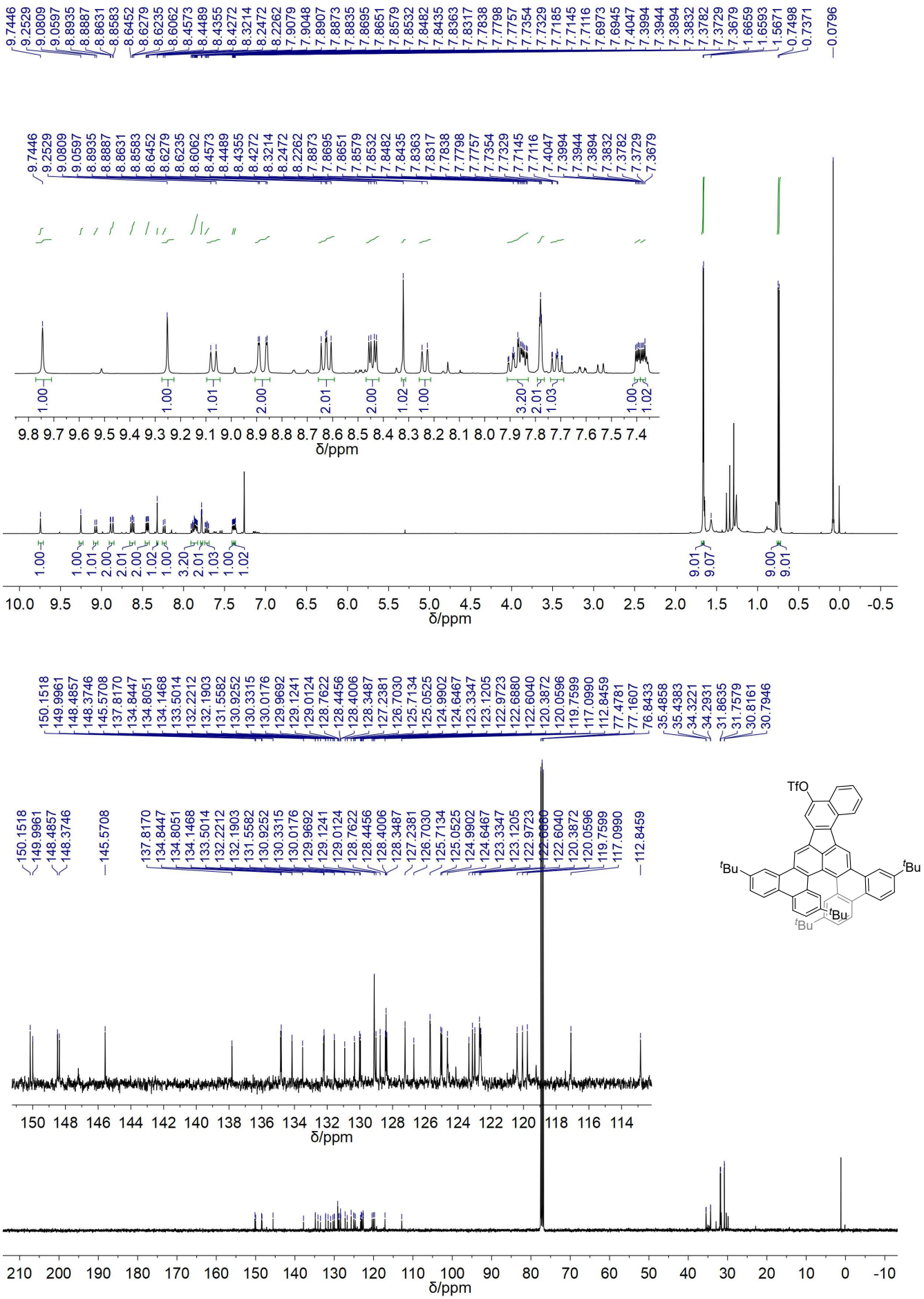

Figure S9. ^{1}H (400 MHz, top) and ^{13}C NMR (101 MHz, bottom) of **3b** in $CDCl_3$ at 25 °C.

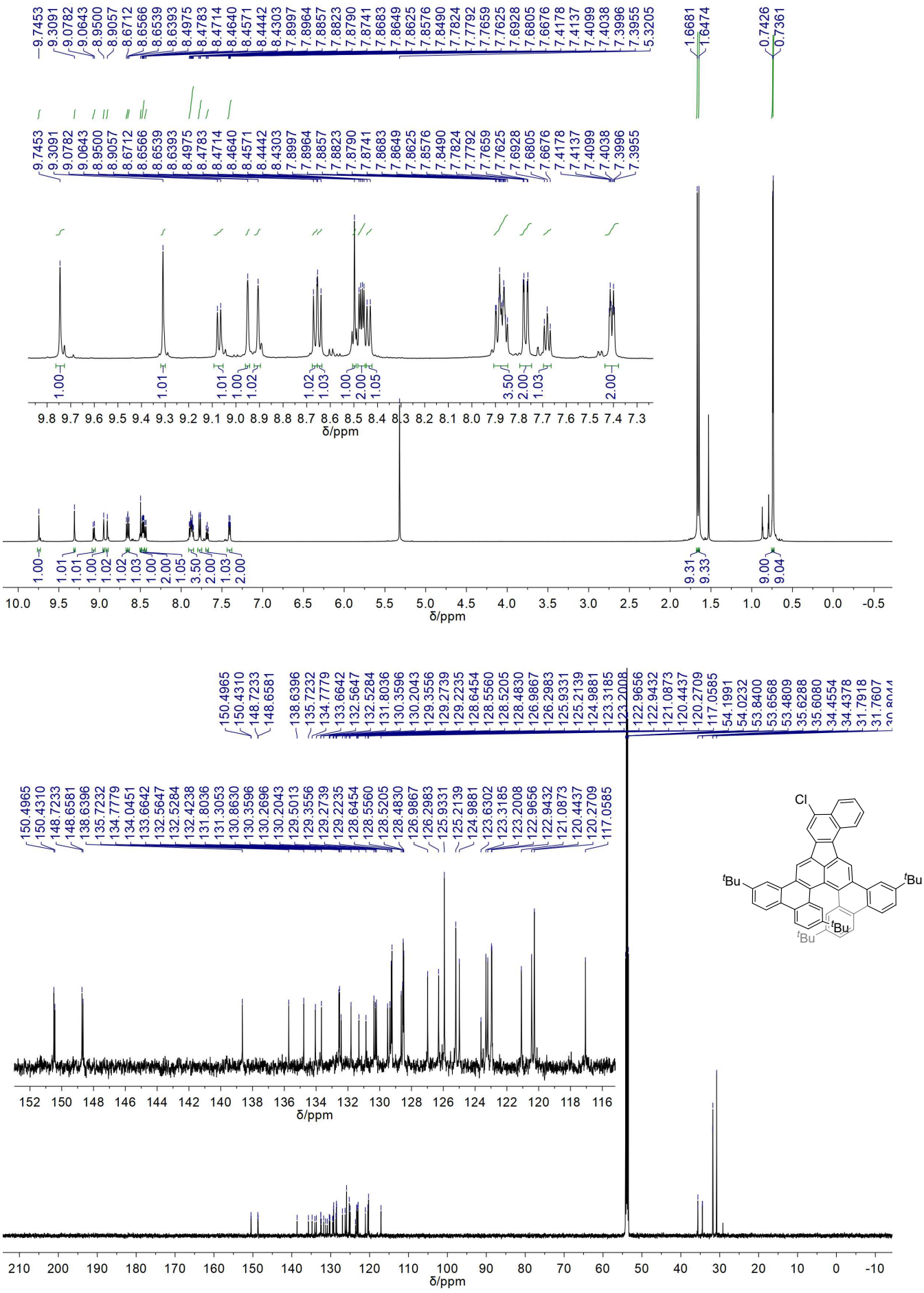

Figure S10. ^{1}H (600 MHz, top) and ^{13}C NMR (150 MHz, bottom) of **3c** in CD_2Cl_2 at 25 °C.

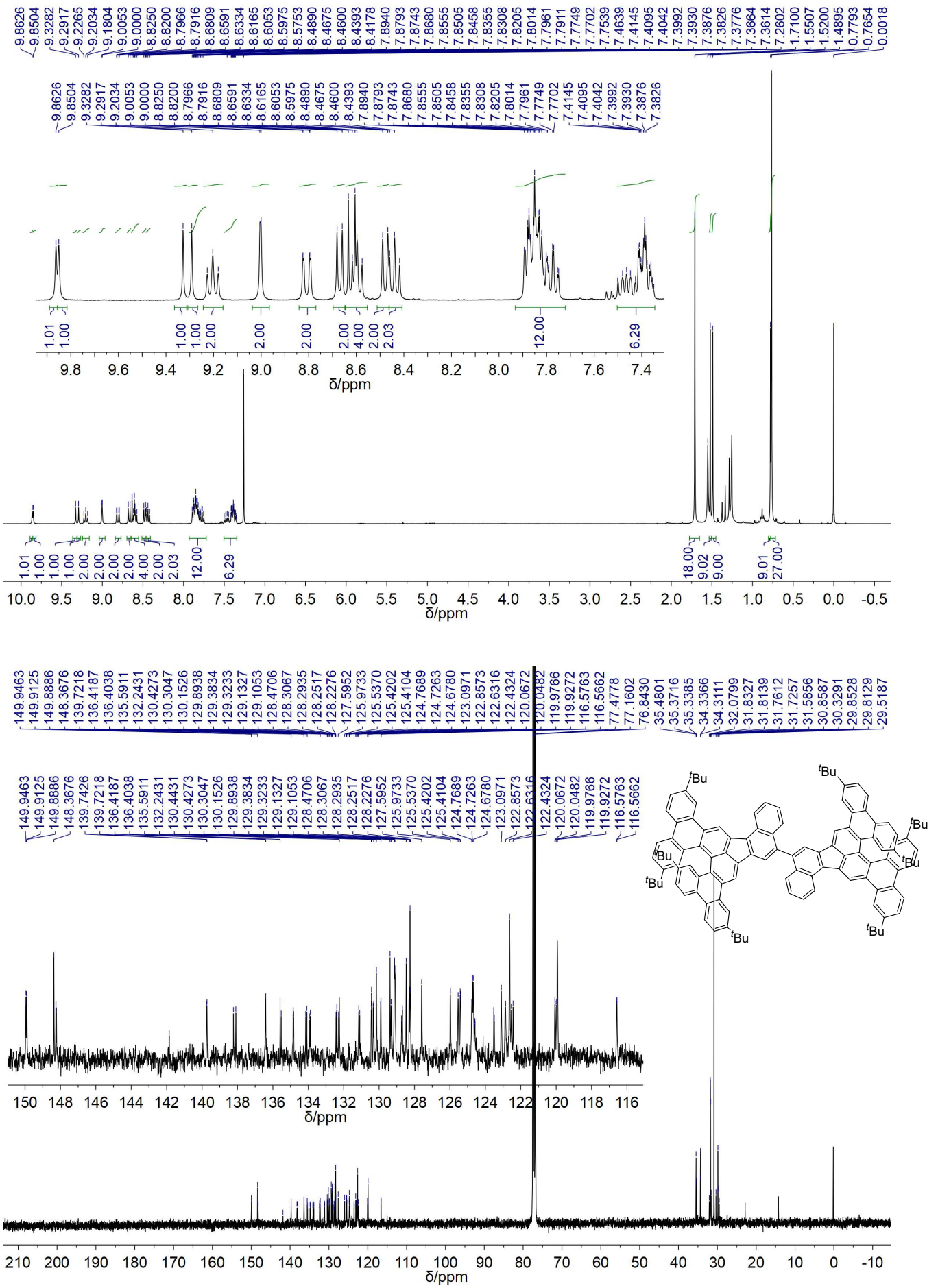

Figure S11. ^{1}H (400 MHz, top) and ^{13}C NMR (101 MHz, bottom) of **4a** in $CDCl_3$ at 25 °C.

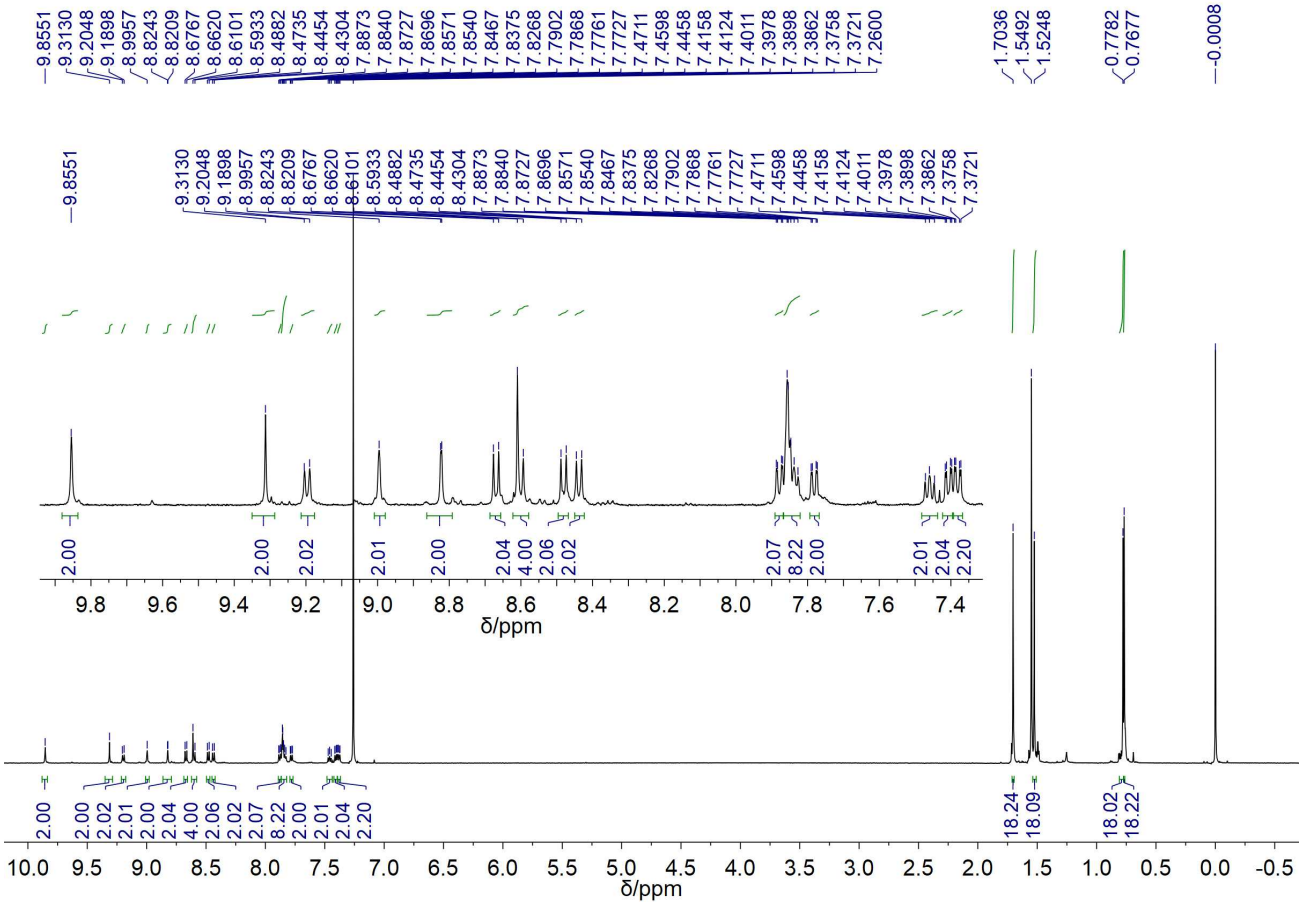

Figure S12. ^{1}H NMR (600 MHz, top) of **4b** in $CDCl_3$ at 25 °C.

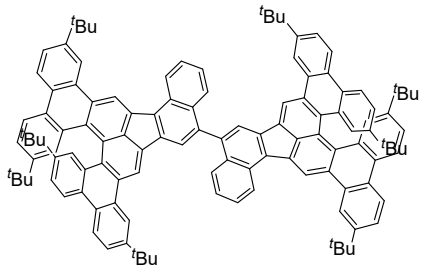

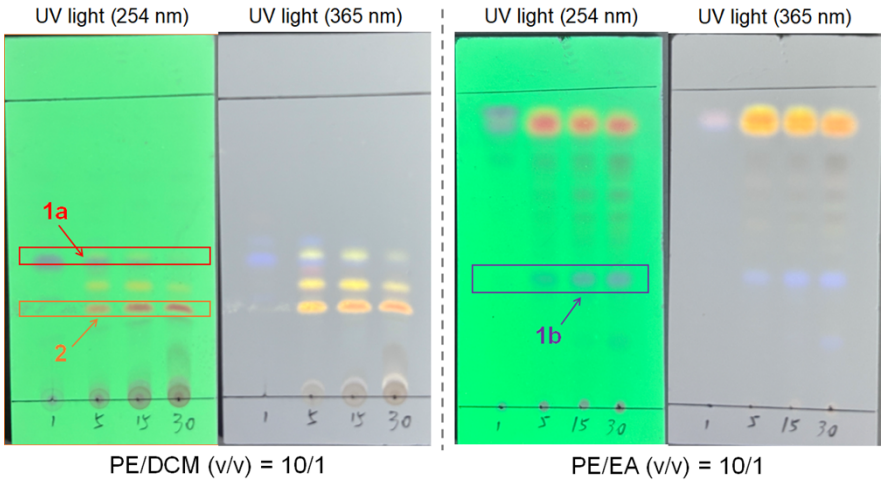

Figure S13. The Scholl reaction of **S1** under the condition of DDQ/$MeSO_3H$ monitored by TLC analysis.

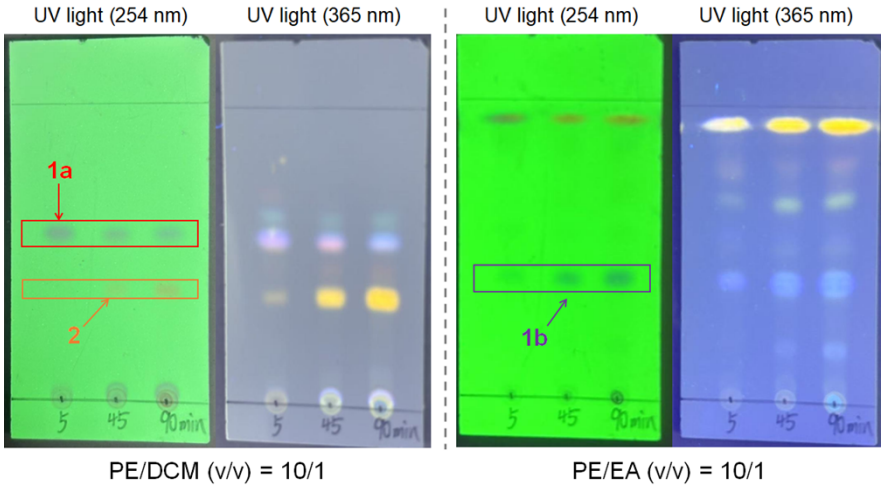

Figure S14. The Scholl reaction of **1a** under the condition of DDQ/$MeSO_3H$ monitored by TLC analysis.

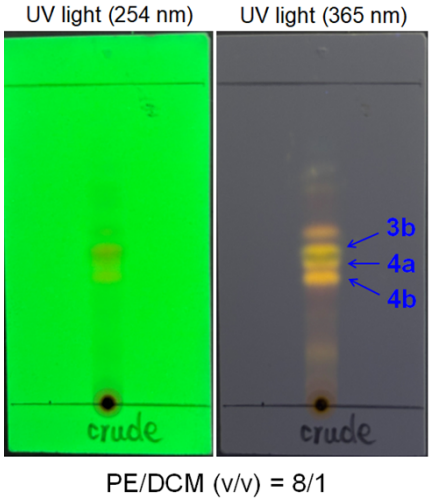

Figure S15. TLC analysis for the Scholl reaction of **S2** under the condition of DDQ/TfOH.

X-ray crystallography

Qualified single crystals of **1a** were obtained by slow vapor diffusion of MeCN into a $CHCl_3$ solution at room temperature. Qualified single crystals of **1c** were obtained by slow vapor diffusion of MeOH into a THF solution at room temperature. Qualified single crystals of **2-rac** were obtained by slow vapor diffusion of MeOH into a $CHCl_3$ solution of the isomeric mixture of **2** upon synthesis at room temperature. Qualified single crystals of **3a** were obtained by slow vapor diffusion of MeCN into a THF solution at room temperature. Qualified single crystals of **3b** were obtained by slow vapor diffusion of MeCN into a $CHCl_3$ solution at room temperature. Qualified single crystals of **3c** were obtained by slow vapor diffusion of MeCN into a $CHCl_3$ solution at room temperature. Qualified single crystals of **4b** were obtained by slow vapor diffusion of MeCN into a $CHCl_3$ solution at room temperature.

Data collection of **1a**, **1c**, **2-rac**, **3a**, **3b**, **3c**, and **4b** were performed on a Bruker D8 VENTURE diffractometer equipped with a metal jet microfocus X-ray source (λ = 1.34139 Å) or a microfocus X-ray source (λ = 0.71073 Å) and a PHOTON M14 detector, under a temperature of 150(2) K (Oxford Cryosystem 1000). The crystal was mounted on a MiTeGen loop with immersion oil. The dataset's reduction and integration were performed with the Bruker software package SAINT (version 8.40B).[2] Data were corrected for absorption effects using the empirical methods as implemented in SADABS (version 2016/2).[3] The structures were solved by SHELXT (version 2018/3)[4] and refined by full-matrix least-squares procedures using the SHELXL (version 2022/12)[5] software package through the Olex2 graphical interface.[6] All non-hydrogen atoms were refined anisotropically. The H-atoms were included at calculated positions and refined as riders, with U_{iso}(H) = 1.2 U_{eq}(C). In each unit cell of **2-rac**, 8.8 chloroform solvent molecules were found to be severely disordered and removed by the Olex2's solvent mask subroutine.[7] The total void volume was 2024 Å^3, equivalent to 22.9% of the unit cell's total volume. In each unit cell of **3a**, 6.4 THF solvent molecule was found to be severely disordered and removed by the Olex2's solvent mask subroutine.[7] The total void volume was 1412 Å^3, equivalent to 14.5% of the unit cell's total volume. In each unit cell of **3b**, 5.4 chloroform solvent molecule was found to be severely disordered and removed by the Olex2's solvent mask subroutine.[7] The total void volume was 1174 Å^3, equivalent to 21.0% of the unit cell's total volume. In each unit cell of **3c**, 1.5 acetonitrile solvent molecule was found to be severely disordered and removed by the Olex2's solvent mask subroutine.[7] The total void volume was 372 Å^3, equivalent to 7.4% of the unit cell's total volume. In each unit cell of **4b**, 5 THF solvent molecule was found to be severely disordered and removed by the Olex2's solvent mask subroutine.[7] The total void volume was 843 Å^3, equivalent to 16.8% of the unit cell's total volume. Crystallographic data and details

of the data collection and structure refinement are listed in Table S1.

Crystallographic data were deposited in the Cambridge Crystallographic Data Centre. The data can be obtained free of charge from The Cambridge Crystallographic Data Centre via www.ccdc.cam.ac.uk/data_request/cif.

Table S1. Crystallographic data and structure refinement parameters.

Compound	**1a**	**1c**	**2-rac**	**3a**
CCDC number	2502680	2502683	2502685	2502686
Empirical formula	$C_{50}H_{52}$	$C_{50}H_{51}Cl$	$C_{102.2}H_{106.6}Cl_{6.6}$	$C_{63.2}H_{60.4}O_{2.8}$
Formula weight	652.91	687.35	1568.84	864.71
Temperature (K)	150(2)	150(2)	150(2)	150(2)
Wavelength (Å)	1.34139	1.34139	1.34139	1.34139
Crystal system	Monoclinic	Orthorhombic	Monoclinic	Monoclinic
Space group	*C*2/*c*	*Pca*2$_1$	*P*2$_1$/*c*	*P*2$_1$/*c*
a (Å)	26.597(3)	13.2085(7)	15.7391(9)	21.6314(13)
b (Å)	13.9495(14)	28.3413(16)	15.8541(8)	15.0244(9)
c (Å)	10.2224(11)	10.7327(6)	36.1543(19)	30.3104(18)
α (°)	90	90	90	90
β (°)	95.212(6)	90	102.015(2)	99.150(2)
γ (°)	90	90	90	90
V (Å^3)	3777.0(7)	4017.7(4)	8823.9(8)	9725.5(10)
Z	4	4	4	8
ρ_{calcd} (g·cm^{-3})	1.148	1.136	1.181	1.181
μ (mm^{-1})	0.319	0.720	1.513	0.359
F(000)	1408	1472	3328	3696
Crystal size (mm)	0.02×0.06×0.08	0.02×0.05×0.15	0.02×0.05×0.1	0.02×0.04×0.1
θ range for data collection (°)	2.903-56.965	3.211-63.556	2.950-52.981	1.800-54.015
Reflections collected	18450	44210	74106	96318
Independent reflections	3857 [R_{int} = 0.0891]	8547 [R_{int} = 0.1035]	15535 [R_{int} = 0.1205]	17861 [R_{int} = 0.0708]
Transmission factors (min/max)	0.5820/0.7536	0.6091/0.7523	0.6316/0.7505	0.6316/0.7505
Data/restraints/parameters	3857/106/274	8547/28/504	15535/1146/1107	17861/1027/1212
*R*1,[a] *wR*2[b] ($I > 2\sigma(I)$)	0.0533, 0.1357	0.0611, 0.1756	0.1308, 0.3640	0.0615, 0.1529
*R*1,[a] *wR*2[b] (all data)	0.0728, 0.1479	0.0804, 0.1789	0.2036, 0.4065	0.0938, 0.1733
Quality-of-fit[c]	1.068	1.074	1.038	1.014

$R_{int} = \Sigma|F_o^2 - \langle F_o^2 \rangle|/\Sigma|F_o^2|$

[a]$R_1 = \Sigma||F_o| - |F_c||/\Sigma|F_o|$. [b]$wR_2 = [\Sigma[w(F_o^2 - F_c^2)^2]/\Sigma[w(F_o^2)^2]]$.

[c]Quality-of-fit = $[\Sigma[w(F_o^2 - F_c^2)^2]/(N_{obs} - N_{params})]^{1/2}$, based on all data.

Compound	**3b**	**3c**	**4b**
CCDC number	2502682	2502684	2502681
Empirical formula	$C_{62.35}H_{59.05}Cl_{4.05}F_3O_3S$	$C_{123.5}H_{115.25}Cl_2N_{1.75}$	$C_{130}H_{130}O_{2.5}$
Formula weight	1088.97	1694.82	1732.33
Temperature (K)	150(2)	150(2)	150(2)
Wavelength (Å)	0.71073	0.71073	1.34139
Crystal system	Monoclinic	Monoclinic	Triclinic
Space group	$P2_1/n$	$P2_1/n$	P-1
a (Å)	19.166(10)	16.844(4)	15.3360(19)
b (Å)	14.302(7)	14.720(4)	15.666(2)
c (Å)	20.773(10)	20.913(6)	21.989(3)
α (°)	90	90	83.646(4)
β (°)	101.587(14)	104.377(8)	78.595(5)
γ (°)	90	90	76.301(5)
V (Å^3)	5578(5)	5023(2)	5020.0(12)
Z	4	2	2
ρ_{calcd} (g·cm^{-3})	1.297	1.121	1.146
μ (mm^{-1})	0.307	0.115	0.319
F(000)	2276	1805	1860
Crystal size (mm)	0.02×0.05×0.09	0.02×0.08×0.12	0.02×0.08×0.1
θ range for data collection (°)	1.941-25.392	1.965-27.538	2.531-49.649
Reflections collected	34430	62648	69549
Independent reflections	10220 [R_{int} = 0.1416]	11530 [R_{int} = 0.0522]	15312 [R_{int} = 0.076]
Transmission factors (min/max)	0.4229/0.7452	0.6840/0.7456	0.363372/0.750632
Data/restraints/parameters	10220/451/766	11530/907/799	15312/546/1327
$R1$,[a] $wR2$[b] ($I > 2\sigma(I)$)	0.1228, 0.3224	0.0897, 0.2792	0.0997, 0.2881
$R1$,[a] $wR2$[b] (all data)	0.2325, 0.3922	0.1187, 0.3099	0.1799, 0.3231
Quality-of-fit[c]	1.029	1.067	1.130

$R_{int} = \Sigma|F_o^2 - \langle F_o^2 \rangle| / \Sigma|F_o^2|$

[a]$R_1 = \Sigma||F_o| - |F_c|| / \Sigma|F_o|$. [b]$wR_2 = [\Sigma[w(F_o^2 - F_c^2)^2] / \Sigma[w(F_o^2)^2]]$.

[c]Quality-of-fit = $[\Sigma[w(F_o^2 - F_c^2)^2] / (N_{obs} - N_{params})]^{1/2}$, based on all data.

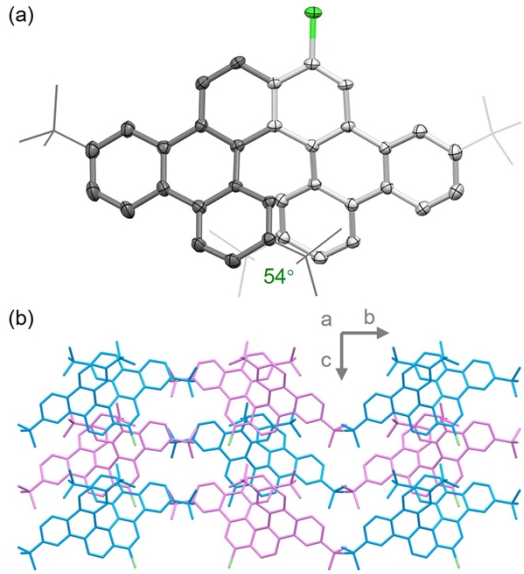

Figure S16. (a) Crystal structure of **1c** in top view, *P*-enantiomer is shown. (b) Packing structure of **1c**, *M*- and *P*-enantiomers are shown in blue and violet, respectively. The thermal ellipsoids are shown at the 50% probability level.

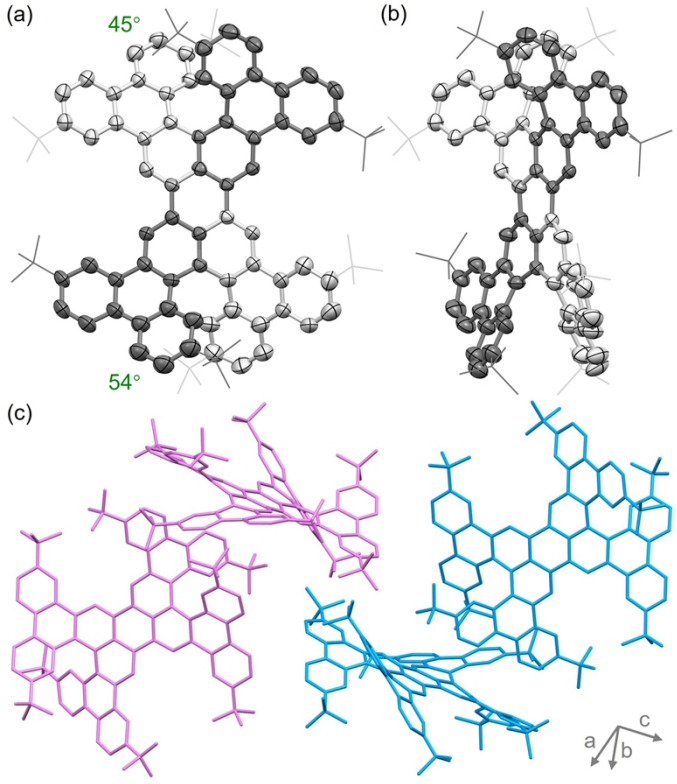

Figure S17. Crystal structure of **2-rac** (a) in top view and (b) in side view, (*P*,*P*)-enantiomer is shown. (c) Packing structure of **2-rac**, (*M*,*M*)- and (*P*,*P*)-enantiomers are shown in blue and violet, respectively. The thermal ellipsoids are shown at the 50% probability level.

The mechanism of the Scholl reaction

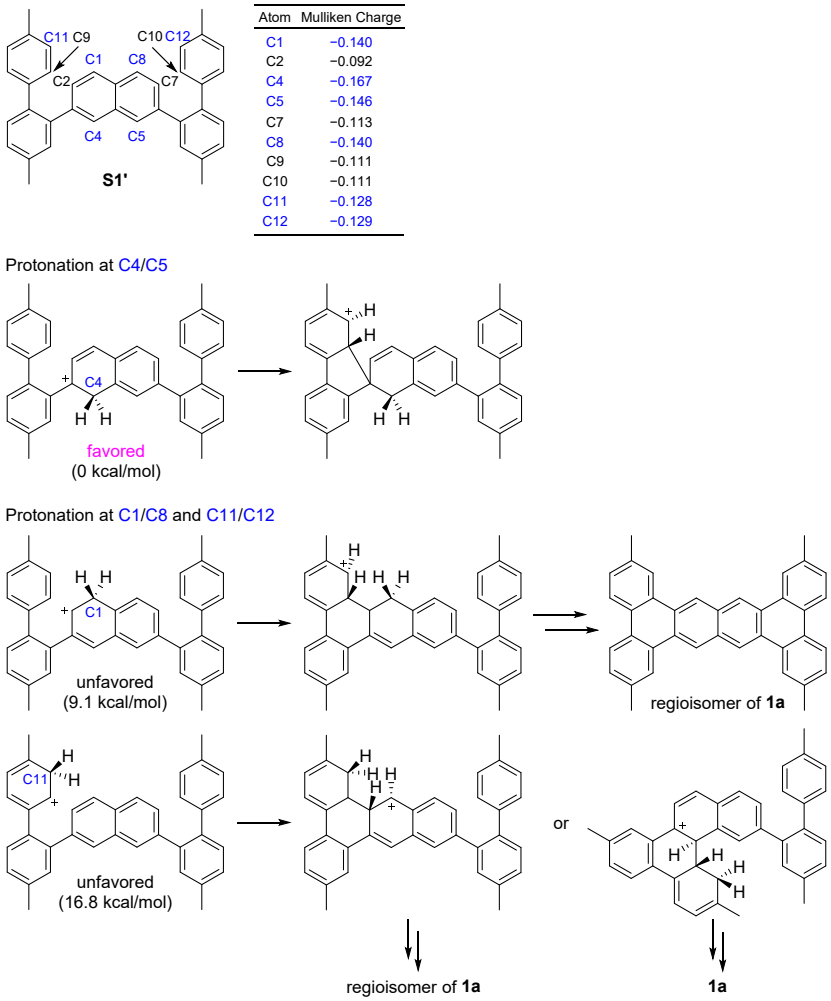

Figure S18. Possible cyclization pathways following the arenium cation mechanism when protonation occurs at position C1/C8, C4/C5, and C11/C12. The computational studies indicate that the arenium cation mechanism cannot be used to explain the Scholl reaction of **S1**.

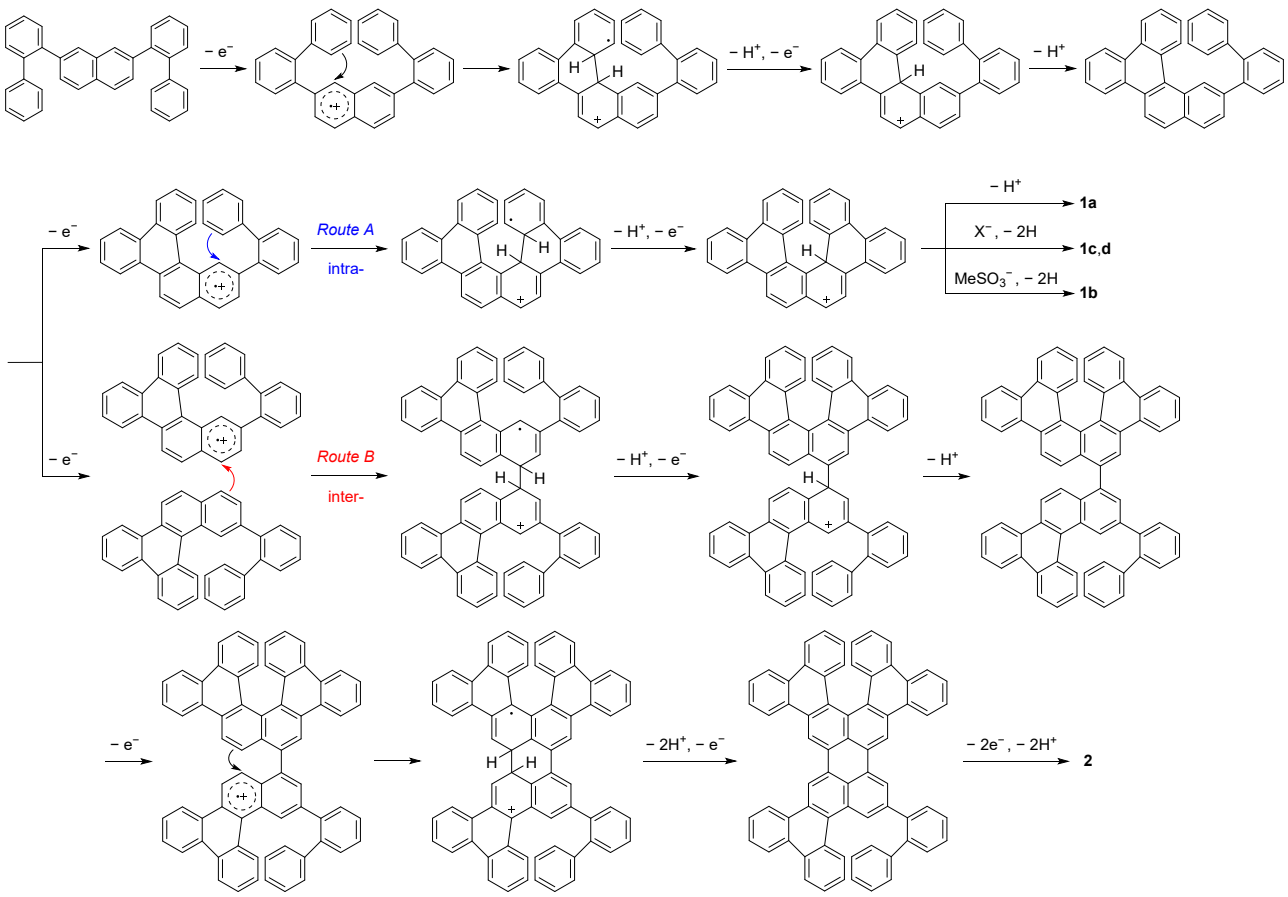

Scheme S4. Proposed mechanism of the Scholl reaction of **S1** through cation radical mechanism. The *tert*-butyl groups are omitted for clarity.

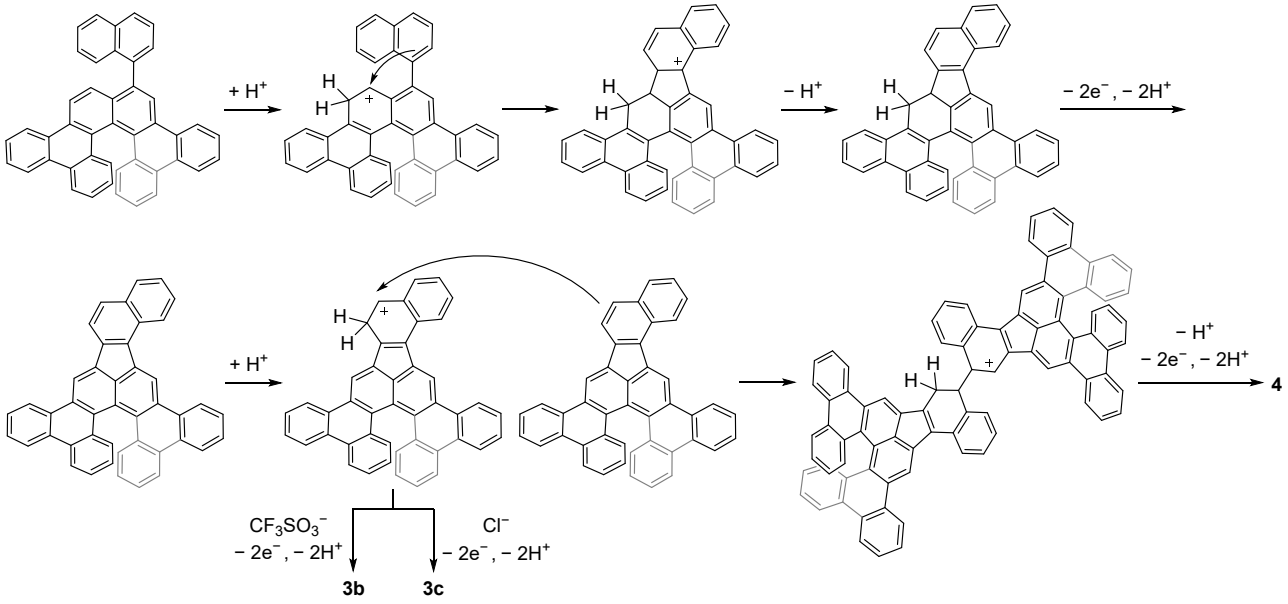

Scheme S5. Proposed mechanism of the Scholl reaction of **S2** through arenium cation mechanism. The *tert*-butyl groups are omitted for clarity.

Thermal isomerization of 4b

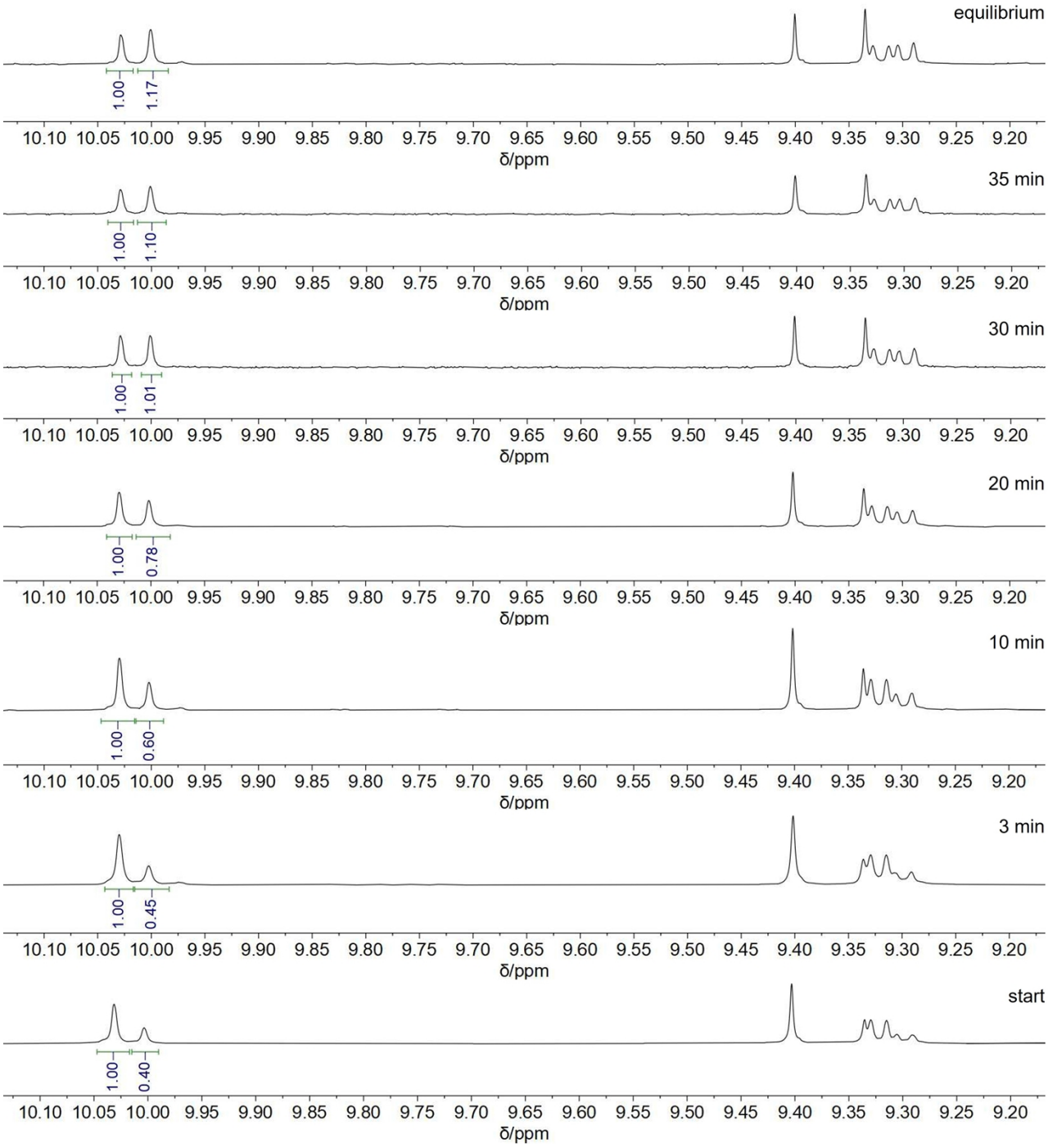

Figure S19. Selected partial ^{1}H NMR spectra of **4b** and **4c** during the progress of thermal isomerization in toluene-d_8 at 45 °C.

Photophysical property

UV-vis absorption spectra were recorded on an Aligent Cary 100 UV-vis spectrophotometer. Emission spectra were recorded on an Aligent Cary Eclipse spectrofluorometer.

The quantum yield of **1a** was determined at the excitation wavelength of 350 nm in $CHCl_3$, and that of **3c**, **4a**, and **4b** were determined at the excitation wavelength of 480 nm in $CHCl_3$, as described by Jobin Yvon Horiba.[8] Quinine sulfate (0.1 M H_2SO_4) and Rhodamine 6G (ethanol) were used as standards. The integrated fluorescence area for **1a** was 450–680 nm, and that for **3c**, **4a**, and **4b** were 500-800 nm. The quantum yield was calculated using the following equation:

$$\Phi_x = \Phi_{std}\left(\frac{Grad_x}{Grad_{std}}\right)\left(\frac{n_x^2}{n_{std}^2}\right)$$

where the subscripts *x* and *std* denote the unknown and the standard, respectively, Φ is the quantum yield, *Grad* is the slope from the plot of integrated fluorescence intensity *versus* absorbance and *n* is the refractive index. The refractive indexes of $CHCl_3$, 0.1 M H_2SO_4, and ethanol are 1.445, 1.332, and 1.3611, respectively.

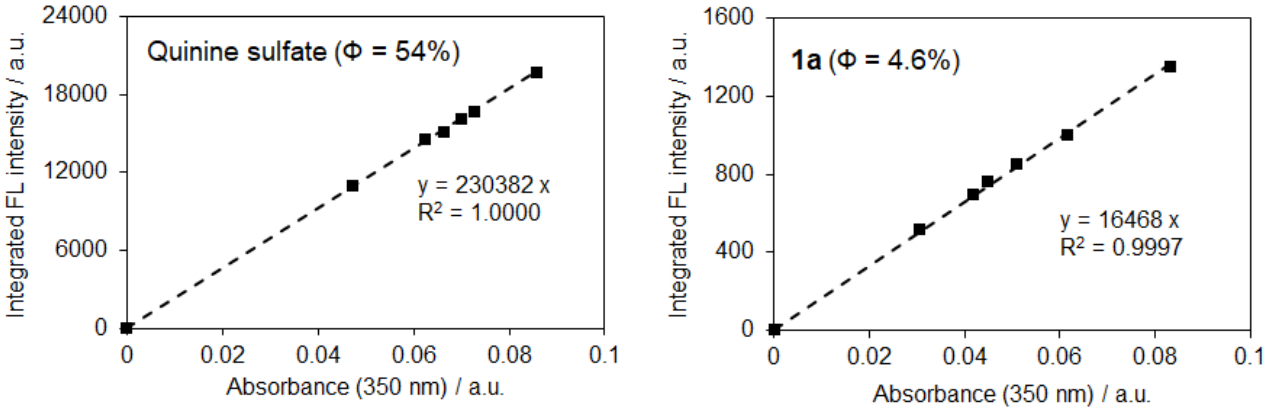

Figure S20. The plots of integrated fluorescence (FL) intensity *versus* absorbance for quinine sulfate and **1a**. The dotted lines are fit to the experimental data (square points).

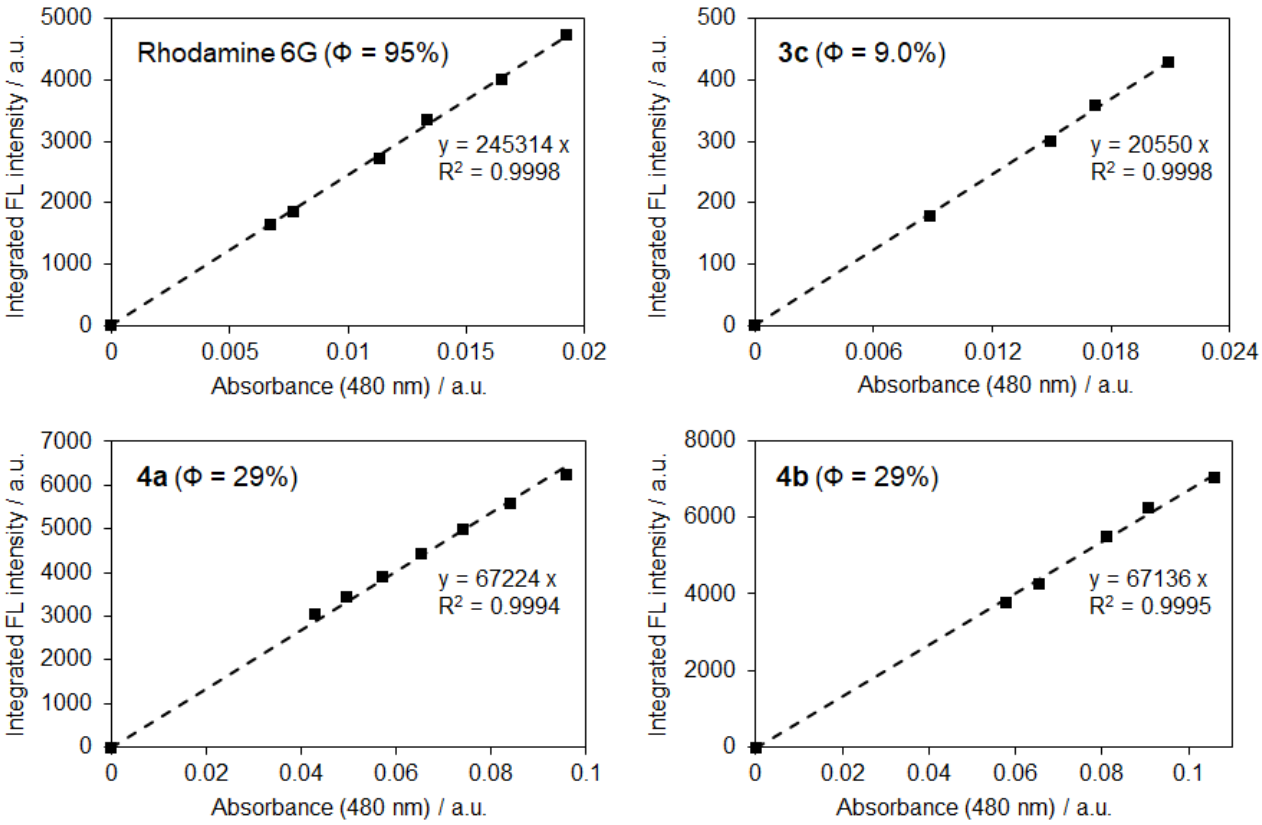

Figure S21. The plots of integrated fluorescence (FL) intensity *versus* absorbance for Rhodamine 6G, **3c**, **4a**, and **4b**. The dotted lines are fit to the experimental data (square points).

DFT calculation

All calculations were performed with Gaussian 16, Revision C.02.[9] The gas-phase geometry was optimized with (U)B3LYP functional[10] and 6-31G(d,p) basis set.[11] Time-dependent DFT (TD-DFT) calculation was performed on optimized structure. Simplified model molecule **S1'**, **S2'**, **1a'**, **2-rac'**, **3c'**, **4a'**, and **4b'**, with methyl groups replacing *tert*-butyl groups in the structure, were used for calculations.

A. Transition state

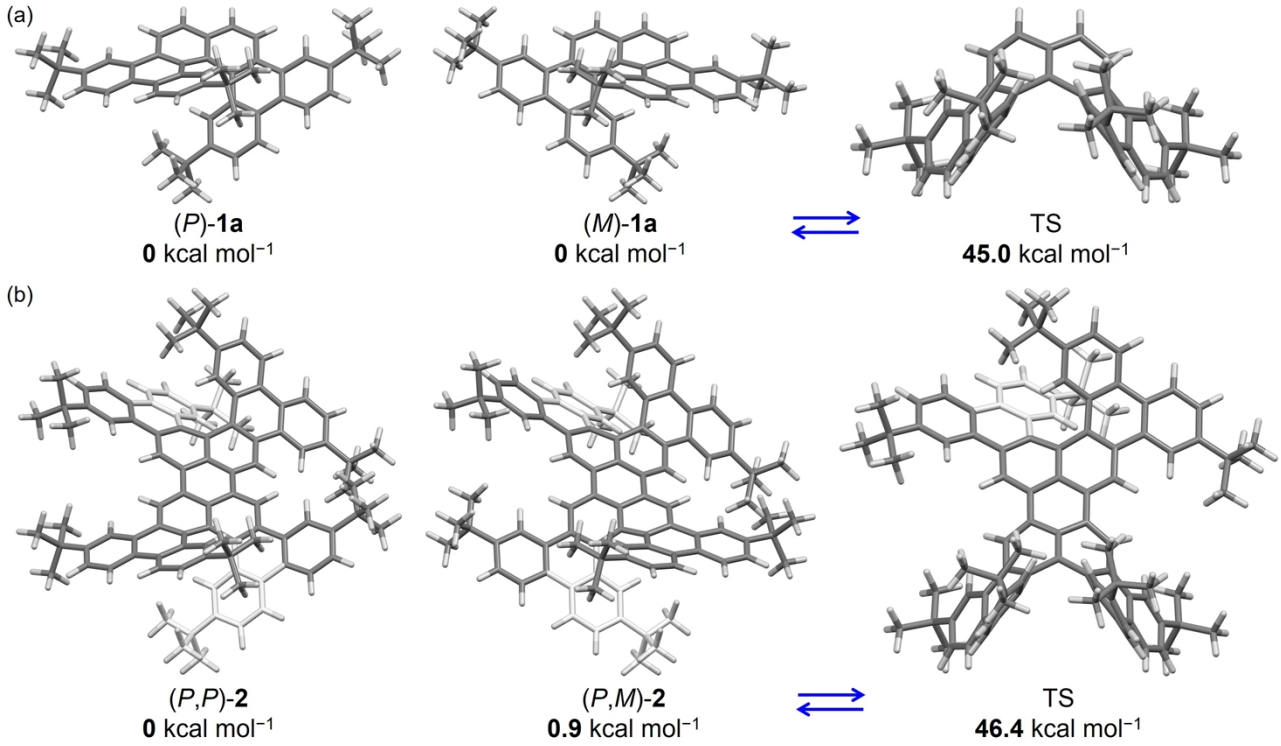

Figure S22. Transition state (TS) between (a) *P*- and *M*-**1a**, and (b) (*P*,*P*)- and (*P*,*M*)-**2**.

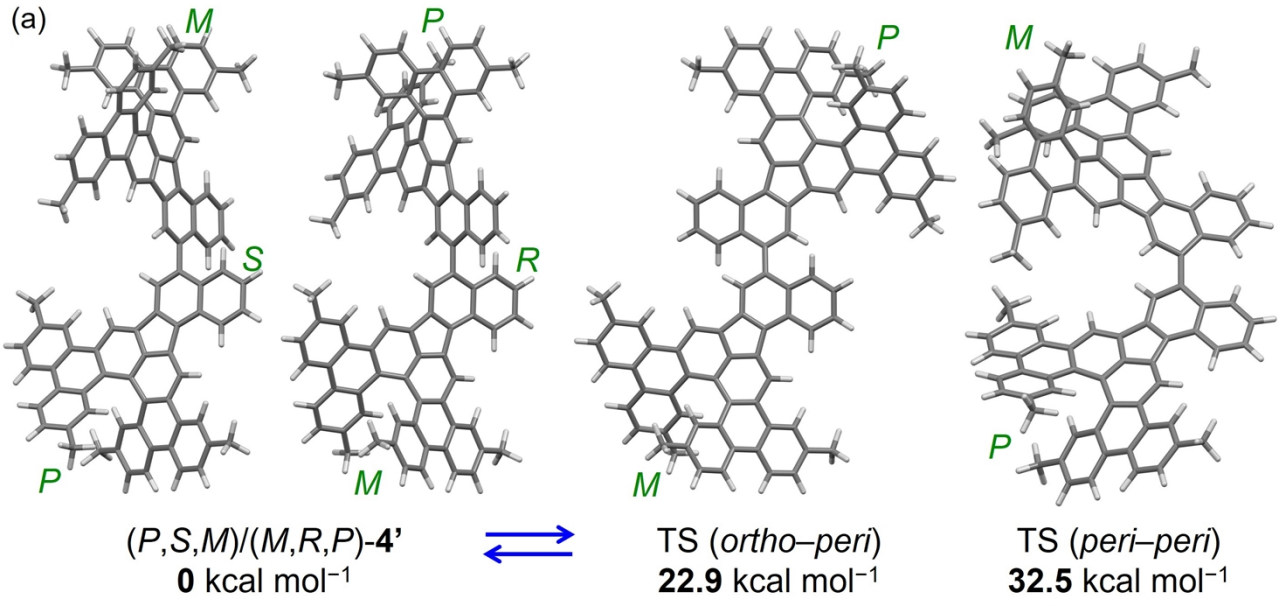

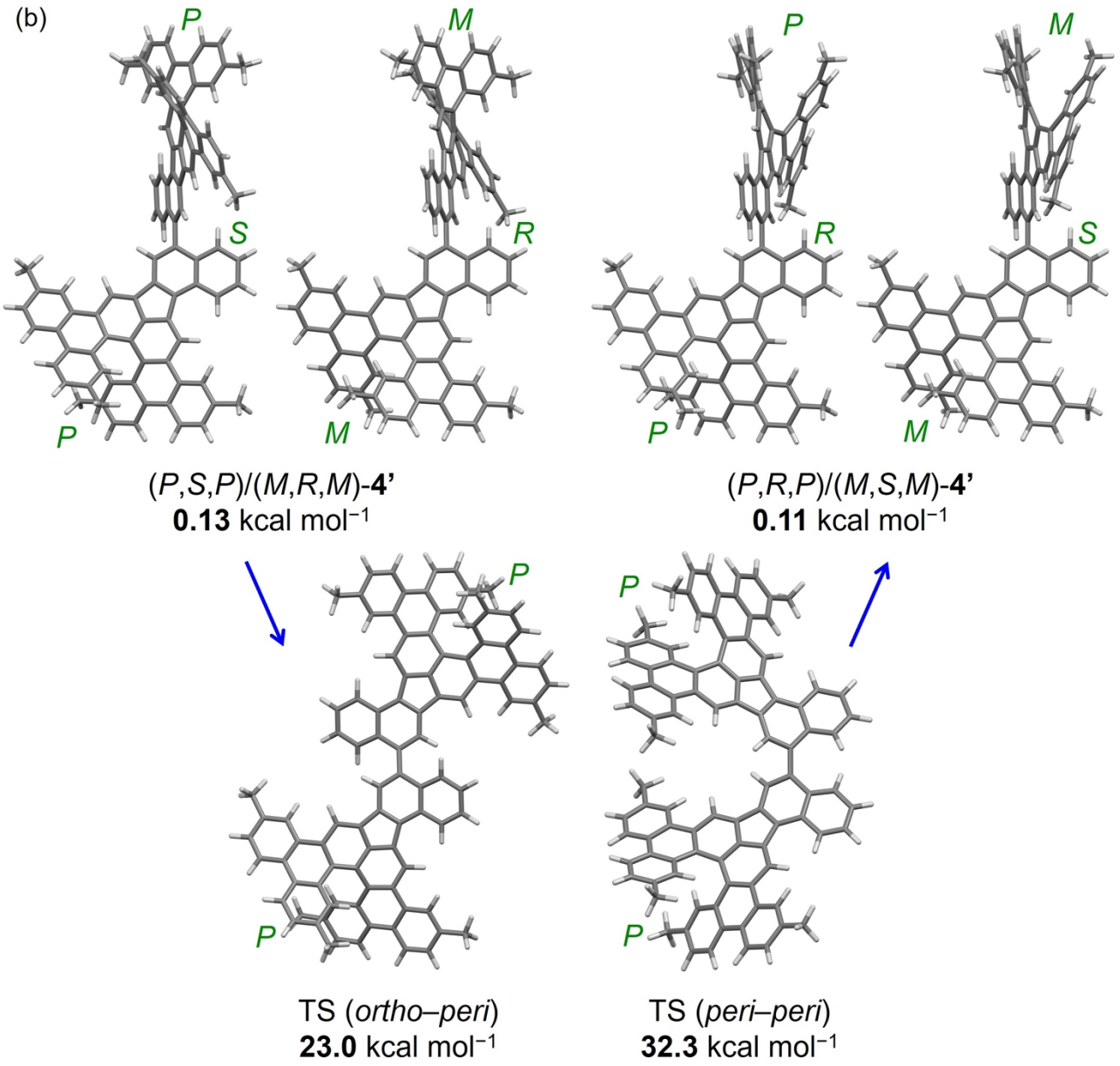

Figure S23. TS between (a) (*P*,*S*,*M*)- and (*M*,*R*,*P*)-**4'**, and (b) (*P*,*S*,*P*)- and (*P*,*R*,*P*)-**4'** through two rotation pathways (*ortho–peri* and *peri–peri* modes).

B. Molecular orbitals

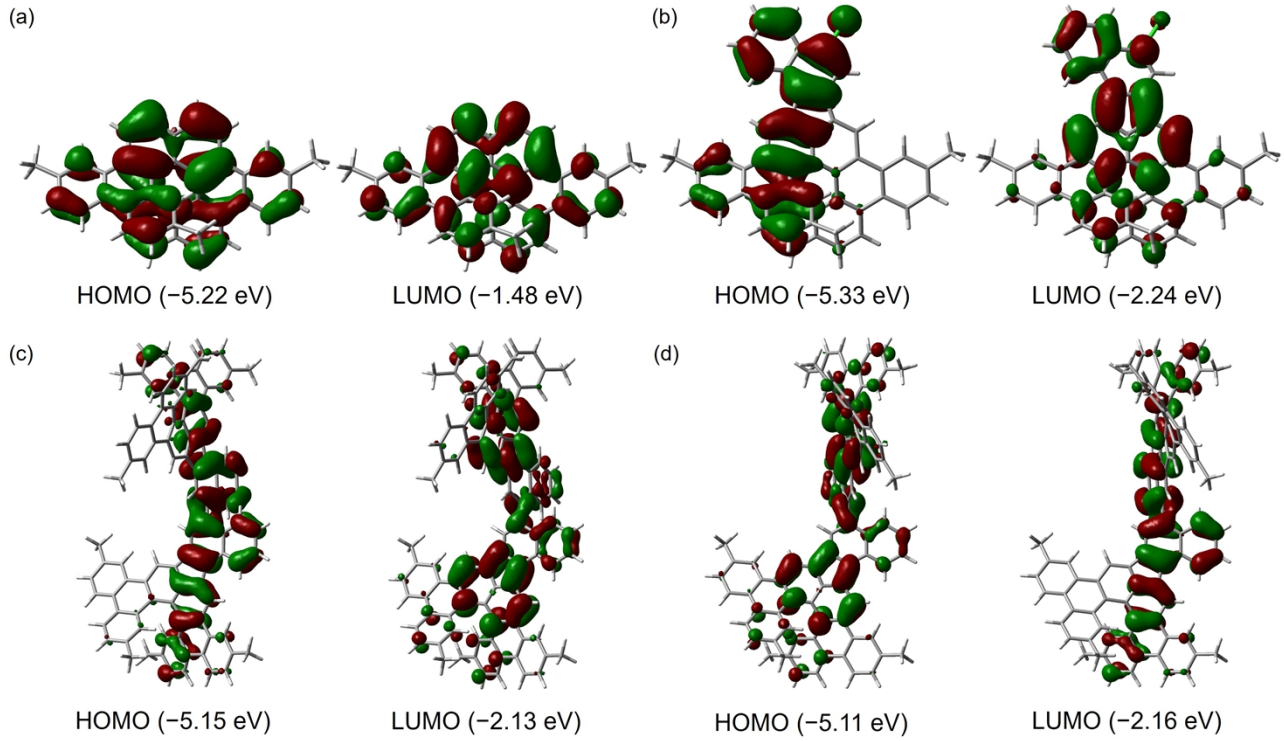

Figure S24. Highest occupied molecular orbital (HOMO) and lowest unoccupied molecular orbital (LUMO) of (a) **1a'**, (b) **3c'**, (c) **4a'**, and (d) **4b'**.

C. Absorption spectrum

Optimized structure of **1a'**, **3c'**, **4a'**, and **4b'** were calculated at the B3LYP/6-31G(d,p) level of DFT. Then, a time-dependent DFT calculation [TD-DFT; CAM-B3LYP/6-31G(d,p)] of 15 states was performed to calculate the UV–Vis spectra.

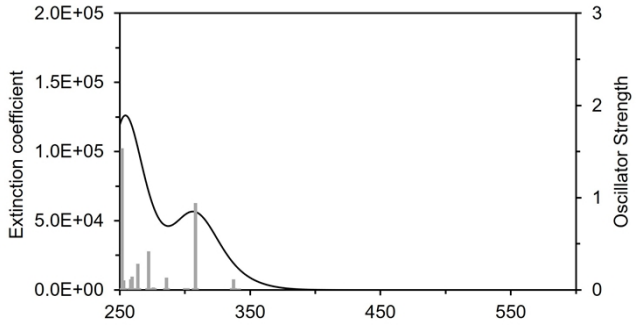

Excited State	Wavelength (nm)	Energy (eV)	Oscillator strength	Major transitions
1	340.41	3.64	0.0005	HOMO → LUMO+1 (0.48) HOMO−1 → LUMO (0.46) HOMO−4 → LUMO (0.12) HOMO−2 → LUMO+3 (0.11)
2	337.18	3.68	0.1138	HOMO → LUMO (0.65) HOMO−1 → LUMO+1 (0.21)
3	307.98	4.03	0.9434	HOMO → LUMO+1 (0.46) HOMO−1 → LUMO (0.45) HOMO−2 → LUMO+3 (0.13) HOMO−3 → LUMO (0.13) HOMO−4 → LUMO (0.12) HOMO → LUMO+4 (0.10)
4	301.06	4.12	0.0036	HOMO−2 → LUMO (0.50) HOMO → LUMO+3 (0.30) HOMO−1 → LUMO+3 (0.27) HOMO−3 → LUMO+1 (0.22) HOMO−3 → LUMO+4 (0.12)

Figure S25. Calculated absorption spectrum and electronic transitions for **1a'**.

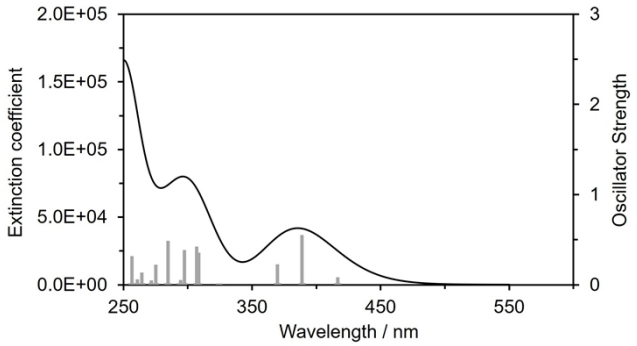

Excited State	Wavelength (nm)	Energy (eV)	Oscillator strength	Major transitions
1	416.78	2.97	0.0818	HOMO → LUMO (0.54) HOMO−1 → LUMO (0.38) HOMO−2 → LUMO (0.18)
2	388.86	3.19	0.5503	HOMO−1 → LUMO (0.55) HOMO → LUMO (0.40)
3	369.76	3.35	0.2275	HOMO−2 → LUMO (0.59) HOMO−1 → LUMO (0.16) HOMO−5 → LUMO (0.15) HOMO → LUMO+1 (0.12) HOMO → LUMO (0.12) HOMO−1 → LUMO+1 (0.10)
4	324.37	3.82	0.0011	HOMO−3 → LUMO (0.60) HOMO → LUMO+1 (0.13) HOMO−3 → LUMO+2 (0.12) HOMO−2 → LUMO+3 (0.12) HOMO−1 → LUMO+1 (0.10)
5	308.43	4.02	0.3539	HOMO → LUMO+1 (0.52) HOMO−4 → LUMO (0.25) HOMO−2 → LUMO (0.16) HOMO−1 → LUMO+2 (0.14) HOMO−5 → LUMO (0.12) HOMO−3 → LUMO (0.11) HOMO−6 → LUMO (0.10)
6	308.36	4.04	0.4225	HOMO−1 → LUMO+1 (0.55) HOMO−6 → LUMO (0.20) HOMO−4 → LUMO (0.16) HOMO−3 → LUMO (0.12) HOMO → LUMO+6 (0.11) HOMO−2 → LUMO (0.11) HOMO → LUMO+2 (0.11)

Figure S26. Calculated absorption spectrum and electronic transitions for **3c'**.

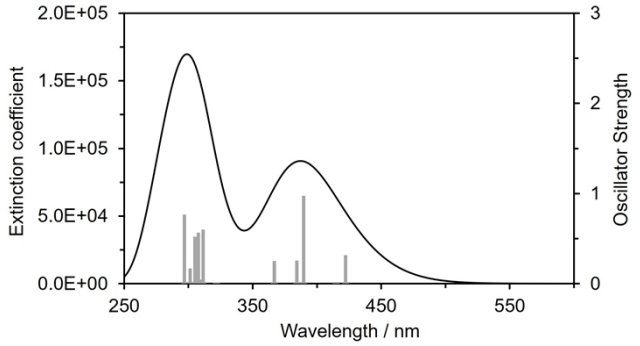

Excited State	Wavelength (nm)	Energy (eV)	Oscillator strength	Major transitions
1	422.38	2.94	0.3174	HOMO → LUMO (0.52) HOMO−3 → LUMO+1 (0.36) HOMO−1 → LUMO+1 (0.22)
2	414.93	2.99	0.0201	HOMO → LUMO+1 (0.46) HOMO−3 → LUMO (0.42) HOMO−2 → LUMO+1 (0.17) HOMO−1 → LUMO (0.16) HOMO−5 → LUMO (0.11)
3	389.70	3.18	0.9742	HOMO−2 → LUMO (0.47) HOMO−1 → LUMO+1 (0.41) HOMO−3 → LUMO+1 (0.25) HOMO → LUMO (0.11)
4	384.27	3.23	0.2552	HOMO−1 → LUMO (0.45) HOMO−2 → LUMO+1 (0.43) HOMO → LUMO+1 (0.19) HOMO−3 → LUMO (0.18)
5	366.88	3.38	0.2536	HOMO−4 → LUMO (0.39) HOMO−5 → LUMO+1 (0.32) HOMO−4 → LUMO+1 (0.26) HOMO−5 → LUMO (0.16) HOMO−1 → LUMO+3 (0.12) HOMO−3 → LUMO+1 (0.12) HOMO−11→ LUMO (0.11) HOMO−10→ LUMO+1(0.11) HOMO−2 → LUMO+2 (0.10)
6	366.74	3.38	0.1726	HOMO−5 → LUMO (0.39) HOMO−4 → LUMO+1 (0.32) HOMO−5 → LUMO+1 (0.26) HOMO−4 → LUMO (0.16) HOMO−3 → LUMO (0.12) HOMO−1 → LUMO+2 (0.12) HOMO−11→ LUMO+1(0.11) HOMO−10→ LUMO (0.11) HOMO−2 → LUMO+3 (0.11) HOMO → LUMO+1 (0.10)
7	321.90	3.85	0.0003	HOMO−6 → LUMO (0.40) HOMO−6 → LUMO+1 (0.39) HOMO → LUMO+3 (0.14) HOMO−7 → LUMO+1 (0.11) HOMO−7 → LUMO (0.10) HOMO−4 → LUMO+6 (0.10)
8	321.85	3.85	0.0010	HOMO−7 → LUMO (0.40) HOMO−7 → LUMO+1 (0.39) HOMO → LUMO+2 (0.14) HOMO−6 → LUMO+1 (0.11) HOMO−5 → LUMO+6 (0.10) HOMO−3 → LUMO+3 (0.10)
9	311.41	3.98	0.6007	HOMO−3 → LUMO+1 (0.28) HOMO → LUMO+2 (0.25) HOMO−3 → LUMO+3 (0.24) HOMO → LUMO (0.24) HOMO−2 → LUMO+2 (0.19) HOMO−9 → LUMO (0.18) HOMO−1 → LUMO+1 (0.16) HOMO → LUMO+4 (0.16)
10	309.14	4.01	0.0464	HOMO−1 → LUMO+2 (0.27) HOMO → LUMO+3 (0.27) HOMO → LUMO+1 (0.22) HOMO−9 → LUMO+1 (0.21) HOMO−3 → LUMO (0.20) HOMO−1 → LUMO (0.15) HOMO−2 → LUMO+3 (0.14) HOMO−8 → LUMO (0.14)
11	307.66	4.03	0.5681	HOMO−1 → LUMO+3 (0.37) HOMO−2 → LUMO+2 (0.27) HOMO → LUMO+2 (0.26) HOMO−8 → LUMO+1 (0.20) HOMO−9 → LUMO (0.19) HOMO−4 → LUMO (0.11) HOMO−5 → LUMO+1 (0.11)
12	305.24	4.06	0.5218	HOMO−2 → LUMO+3 (0.36) HOMO−3 → LUMO+2 (0.27) HOMO−1 → LUMO+2 (0.25) HOMO−12→ LUMO (0.15) HOMO−3 → LUMO (0.14) HOMO → LUMO+1 (0.12) HOMO−13→ LUMO+1(0.12) HOMO−5 → LUMO (0.11) HOMO−2 → LUMO+2 (0.11)
13	302.83	4.09	0.0050	HOMO → LUMO+1 (0.36) HOMO−3 → LUMO (0.31) HOMO−1 → LUMO (0.23) HOMO → LUMO+3 (0.20) HOMO−8 → LUMO (0.19) HOMO−10→ LUMO (0.13) HOMO−3 → LUMO+2 (0.11)
14	301.31	4.11	0.1698	HOMO−2 → LUMO+2 (0.25) HOMO−3 → LUMO+3 (0.25) HOMO → LUMO (0.25) HOMO−3 → LUMO+1 (0.22) HOMO−1 → LUMO+1 (0.19) HOMO−9 → LUMO (0.16) HOMO−13→ LUMO (0.14) HOMO−11→ LUMO (0.14) HOMO−12→ LUMO+1(0.11) HOMO−1 → LUMO+3 (0.11)

Figure S27. Calculated absorption spectrum and electronic transitions for **4a'**.

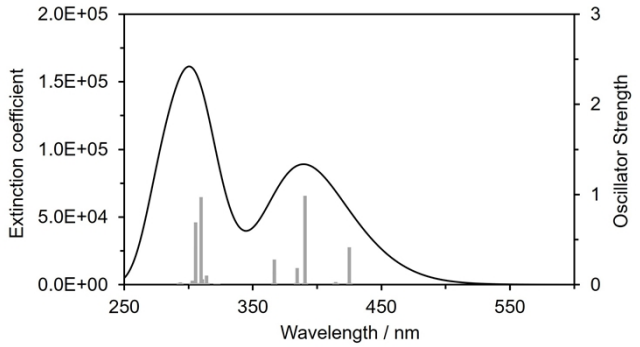

Excited State	Wavelength (nm)	Energy (eV)	Oscillator strength	Major transitions
1	425.18	2.92	0.4153	HOMO → LUMO (0.53) HOMO−3 → LUMO+1 (0.39) HOMO−1 → LUMO (0.12) HOMO−5 → LUMO+1 (0.10)
2	414.57	2.99	0.0281	HOMO−3 → LUMO (0.45) HOMO → LUMO+1 (0.44) HOMO−1 → LUMO+1 (0.21) HOMO−5 → LUMO (0.13) HOMO−4 → LUMO+1 (0.10)
3	390.56	3.17	0.9876	HOMO−1 → LUMO (0.48) HOMO−2 → LUMO+1 (0.45) HOMO → LUMO (0.16)
4	384.44	3.23	0.1860	HOMO−2 → LUMO (0.49) HOMO−1 → LUMO+1 (0.41) HOMO → LUMO+1 (0.24)
5	366.77	3.38	0.2789	HOMO−4 → LUMO (0.43) HOMO−5 → LUMO+1 (0.40) HOMO−2 → LUMO+3 (0.13) HOMO−10→ LUMO (0.12) HOMO−3 → LUMO+1 (0.11) HOMO−1 → LUMO+2 (0.10)
6	366.76	3.38	0.1416	HOMO−5 → LUMO (0.43) HOMO−4 → LUMO+1 (0.41) HOMO−3 → LUMO (0.12) HOMO−2 → LUMO+2 (0.12) HOMO−10→ LUMO+1(0.11) HOMO−1 → LUMO+3 (0.11) HOMO−11→ LUMO (0.10)
7	322.01	3.85	0.0007	HOMO−6 → LUMO (0.42) HOMO−7 → LUMO+1 (0.39) HOMO−3 → LUMO+3 (0.15) HOMO → LUMO+2 (0.15)
8	321.93	3.85	0.0006	HOMO−7 → LUMO (0.42) HOMO−6 → LUMO+2 (0.40) HOMO−3 → LUMO+2 (0.14) HOMO → LUMO+1 (0.14)
9	314.04	3.95	0.1034	HOMO−8 → LUMO (0.36) HOMO−3 → LUMO+1 (0.36) HOMO → LUMO (0.25) HOMO → LUMO+4 (0.16) HOMO−1 → LUMO+2 (0.14) HOMO−2 → LUMO+3 (0.14) HOMO−10→ LUMO (0.13) HOMO−9 → LUMO+1 (0.12) HOMO−11→ LUMO+1(0.10)
10	310.92	3.99	0.0582	HOMO−3 → LUMO (0.31) HOMO → LUMO+1 (0.30) HOMO−8 → LUMO+1 (0.27) HOMO → LUMO+3 (0.19) HOMO−3 → LUMO+2 (0.17) HOMO−2 → LUMO+2 (0.16) HOMO−1 → LUMO+3 (0.11) HOMO−7 → LUMO (0.10)
11	309.71	4.00	0.9714	HOMO → LUMO+2 (0.42) HOMO−3 → LUMO+3 (0.30) HOMO−6 → LUMO (0.15) HOMO−7 → LUMO+1 (0.15) HOMO−12→ LUMO (0.14) HOMO−1 → LUMO+2 (0.12) HOMO−13→ LUMO+1(0.11) HOMO−1 → LUMO+4 (0.10)
12	305.52	4.06	0.6911	HOMO−2 → LUMO+3 (0.39) HOMO−1 → LUMO+2 (0.37) HOMO → LUMO+2 (0.17) HOMO−5 → LUMO+1 (0.15) HOMO−3 → LUMO+1 (0.14) HOMO−4 → LUMO (0.14) HOMO → LUMO (0.12) HOMO−12→ LUMO (0.11)
13	305.41	4.06	0.4179	HOMO−2 → LUMO+2 (0.39) HOMO−1 → LUMO+3 (0.37) HOMO−3 → LUMO (0.17) HOMO−5 → LUMO (0.15) HOMO → LUMO+1 (0.15) HOMO−9 → LUMO (0.11) HOMO → LUMO+3 (0.11) HOMO−4 → LUMO+1 (0.11) HOMO−13→ LUMO (0.10) HOMO−12→ LUMO+1(0.10)
14	302.87	4.09	0.0465	HOMO → LUMO+3 (0.33) HOMO−3 → LUMO+2 (0.28) HOMO → LUMO+1 (0.25) HOMO−3 → LUMO (0.25) HOMO−13→ LUMO (0.14) HOMO → LUMO+5 (0.13) HOMO−12→ LUMO+1(0.12) HOMO−1 → LUMO+3 (0.12) HOMO−7 → LUMO (0.10)

Figure S28. Calculated absorption spectrum and electronic transitions for **4b'**.

Reference

1 Liu, F.; Shen, X.; Wu, Y.; Bai, L.; Zhao, H.; Ba, X. Synthesis of ladder-type graphene ribbon oligomers from pyrene units. *Tetrahedron Lett.* **2016**, *57*, 4157–4161.

2 SAINT; part of Bruker APEX5 software package (version 2023.9-4): Bruker AXS, **2023**.

3 SADABS; part of Bruker APEX5 software package (version 2023.9-4): Bruker AXS, **2023**.

4 Sheldrick, G. M. SHELXT - Integrated Space-Group and Crystal-Structure Determination. *Acta Crystallogr.* **2015**, *A71*, 3–8.

5 Sheldrick, G. M. Crystal Structure Refinement with SHELXL. *Acta Crystallogr.* **2015**, *C71*, 3–8.

6 Dolomanov, O. V.; Bourhis, L. J.; Gildea, R. J.; Howard, J. A. K.; Puschmann, H. OLEX2: A Complete Structure Solution, Refinement and Analysis Program. *J. Appl. Crystallogr.* **2009**, *42*, 339–341.

7 Spek, A. L. PLATON SQUEEZE: A Tool for the Calculation of the Disordered Solvent Contribution to the Calculated Structure Factors. *Acta Crystallogr C*, **2015**, *71*, 9–18.

8 Jobin Yvon Horiba, "A Guide to Recording Fluorescence Quantum Yields". See the link: https://static.horiba.com/fileadmin/Horiba/Application/Materials/Material_Research/Quantum_Dots/quantumyieldstrad.pdf.

9 Gaussian 16, Revision C.02, Frisch, M. J.; Trucks, G. W.; Schlegel, H. B.; Scuseria, G. E.; Robb, M. A.; Cheeseman, J. R.; Scalmani, G.; Barone, V.; Petersson, G. A.; Nakatsuji, H.; Li, X.; Caricato, M.; Marenich, A. V.; Bloino, J.; Janesko, B. G.; Gomperts, R.; Mennucci, B.; Hratchian, H. P.; Ortiz, J. V.; Izmaylov, A. F.; Sonnenberg, J. L.; Williams-Young, D.; Ding, F.; Lipparini, F.; Egidi, F.; Goings, J.; Peng, B.; Petrone, A.; Henderson, T.; Ranasinghe, D.; Zakrzewski, V. G.; Gao, J.; Rega, N.; Zheng, G.; Liang, W.; Hada, M.; Ehara, M.; Toyota, K.; Fukuda, R.; Hasegawa, J.; Ishida, M.; Nakajima, T.; Honda, Y.; Kitao, O.; Nakai, H.; Vreven, T.; Throssell, K.; Montgomery, Jr., J. A.; Peralta, J. E.; Ogliaro, F.; Bearpark, M. J.; Heyd, J. J.; Brothers, E. N.; Kudin, K. N.; Staroverov, V. N.; Keith, T. A.; Kobayashi, R.; Normand, J.; Raghavachari, K.; Rendell, A. P.; Burant, J. C.; Iyengar, S. S.; Tomasi, J.; Cossi, M.; Millam, J. M.; Klene, M.; Adamo, C.; Cammi, R.; Ochterski, J. W.; Martin, R. L.; Morokuma, K.; Farkas, O.; Foresman, J. B.; Fox, D. J. Gaussian, Inc., Wallingford CT, 2016.

10 (a) Kim, K.; Jordan, K. D. Comparison of Density Functional and MP2 Calculations on the Water Monomer and Dimer. *J. Phys. Chem.* **1994**, *98*, 10089–10094. (b) Stephens, P. J.; Devlin, F. J.; Chabalowski, C. F.; Frisch, M. J. Ab Initio Calculation of Vibrational Absorption and Circular Dichroism Spectra Using Density Functional Force Fields. *J. Phys. Chem.* **1994**, *98*, 11623–11627.

11 Ditchfield, R.; Hehre, W. J.; Pople, J. A. Self-Consistent Molecular-Orbital Methods. IX. An Extended Gaussian-Type Basis for Molecular-Orbital Studies of Organic Molecules. *J. Chem. Phys.* **1971**, *54*, 724–728.